AD NUMBER

AD849591

LIMITATION CHANGES

TO:

Approved for public release; distribution is unlimited.

FROM:

**Distribution authorized to U.S. Gov't. agencies and their contractors;
Administrative/Operational Use; AUG 1968. Other requests shall be referred to Army Missile Command, Redstone Arsenal, AL.**

AUTHORITY

MICOM ltr 1 Dec 1972

JPC 448

Report Number
TM-68-6

An Experimental Investigation of the Pressure and Velocity Profiles in a Spinning, Cold-flow Rocket Motor

by

G. R. Johnson

M. R. L'Ecuyer

Contract Number DA-AH01-67-C-2215
U.S. Army Missile Command
Redstone Arsenal
Alabama

August 1968

JET PROPULSION CENTER
PURDUE UNIVERSITY

SCHOOL OF MECHANICAL ENGINEERING
LAFAYETTE, INDIANA

PURDUE UNIVERSITY

AND

PURDUE RESEARCH FOUNDATION

Lafayette, Indiana

Report No. TM-68-6

AN EXPERIMENTAL INVESTIGATION OF THE PRESSURE AND VELOCITY PROFILES IN A SPINNING, COLD-FLOW ROCKET MOTOR

Technical Memorandum

by

G. R. Johnson
M. R. L'Ecuyer

Contract No. DA-AH01-67-C-2215

United States Army Missile Command

Redstone Arsenal, Alabama 35809

attn. AMSMI-RKA.

Jet Propulsion Center

Purdue University

August 1968

ACKNOWLEDGEMENTS

This investigation was supported by the United States Army Missile Command, Redstone Arsenal, Alabama, under Contract Numbers DA-01-021-AMC-15257(Z) and DA-AH01-67-C-2215. The assistance of Mr. William Guthrie, the technical monitor for the contract, was of great benefit to this investigation and his efforts are gratefully acknowledged.

The authors wish to express their gratitide to Dr. B.A. Reese, Director of the Jet Propulsion Center, for his significant contributions to this investigation. Dr. J.D. Hoffman is gratefully acknowledged for his helpful discussions throughout the investigation.

The authors also would like to express their sincere appreciation to Mr. B.W. Farquhar and Mr. W.M. Stanley, Research Assistants, for their assistance throughout this investigation.

TABLE OF CONTENTS

LIST OF TABLES

LIST OF FIGURES

LIST OF NOMENCLATURE

d	inside diameter of probe orifice
D	outside diameter of probe orifice
H	total pressure
K_n	calibration factor for n^{th} port
p	static pressure
p_{atm}	atmospheric pressure
p_n	pressure sensed in n^{th} port
q	dynamic pressure
r	radius
R_w	wall radius
U	axial velocity component
V_r	radial velocity component
V_θ	tangential velocity component
V	velocity

Greek symbols

θ	pitch angle
ψ	yaw angle
ϕ	swirl angle $[\phi = \arctan V/U]$
ω_o	angular velocity
ρ	density

ABSTRACT

An experimental investigation was conducted to examine the flow field within the chamber of a spinning, cold-flow rocket motor. The subject investigation was divided into two phases: (1) the selection and calibration of a suitable probe and (2) pressure and velocity measurements within the chamber of the cold-flow apparatus.

A five-port impact tube probe was selected and calibrated. The three-dimensional calibration scheme employed for the subject investigation did not require the probe to be rotated once positioned within the rocket motor chamber.

Experiments were conducted in the rocket motor chamber when a 1.125 inch throat diameter nozzle and a 2.0 inch throat diameter nozzle were employed. Pressure and velocity profiles were measured at two longitudinal locations within the chamber for rotational speeds of 1000, 3000 and 5000 rpm.

The measured axial and tangential velocity profiles were compared with the predicted axial and tangential velocity profiles which were based upon a uniform axial velocity injection and a solid body vortex. The agreement of the experimental data and the predicted

values was excellent when the ratio of the maximum tangential velocity to the axial velocity was approximately 1.6 or less. However, when this ratio was greater than 1.6, the measured velocity profiles differed substantially from the predicted profiles. Mechanisms to explain these results are discussed.

1. INTRODUCTION

A problem of considerable experimental and theoretical interest is the description of the interior ballistics of a spinning, solid-propellant rocket motor. This interest has developed since the use of spin stabilized, solid-propellant rocket motors has shown that the actual performance under spinning conditions differed substantially from the performance predicted from non-spinning, solid-propellant rocket motor data.

An extensive program was undertaken at the Jet Propulsion Center, Purdue University in an effort to improve the understanding of the effects of spin upon the ballistic performance of a solid-propellant rocket motor. This program was divided into two parts: an analytical study by Norton et al. (1967) (1 and 2)* to develop a technique for predicting the performance of spinning, solid-propellant rocket motors, and a cold-flow experimental study conducted by Farquhar et al. (1967) (3) to study the effects of rotation on the internal ballistics of the motor.

The purpose of the research, the results of which are presented herein, was to study the effects of rotation on the flow field inside

---

* Numbers in parentheses refer to references listed in the BIBLIOGRAPHY. Preceding many of the references will be the date the article was published, also in parentheses.

the chamber of the simulated end-burning motor. In particular, the cold-flow study offered the possibility of the use of flow probes for determining the axial velocity component, the tangential velocity component, the radial velocity component and the static pressure profiles within the chamber of the spinning, cold-flow rocket motor. It was hoped that these velocity and pressure profiles within the chamber could provide some useful information about the flow phenomena in a rotating rocket motor.

The subject investigation consisted of two phases:

(1) the selection and calibration of a suitable probe for the pressure and velocity measurements

(2) the pressure and velocity measurements within the chamber of the spinning, cold-flow rocket motor.

Chapters 1, 2 and 3 are concerned with the selection and calibration of the probe employed in the subject investigation. Chapters 4 and 5 are concerned with the application of the probe for the pressure and velocity measurements within the chamber of the spinning, cold-flow rocket motor.

Prior to selecting a suitable probe, a brief review of the literature on swirling flows was conducted to obtain some insight into the nature of the swirling flow phenomena. This review included an introduction to the techniques which have been successfully employed for fluid-flow measurements in a swirling flow. The various measurement techniques which were considered for the subject investigation are described in greater detail in Section 1.3. The

literature reviewed in Section 1.1 is limited to recent experimental studies and does not include studies that are solely analytical. Norton et al. (1967) (1) includes a general review of the analytical studies of swirling flow phenomena.

1.1 Measurements in a Swirling Flow

Several authors (4), (5), (6), (7) and (8) have presented articles on fluid measurements in swirling flows. These studies have, in general, been confined to vortex tubes and pipe flow. These systems have employed tangential or near tangential injection, or adjustable vanes to impart a swirl component to the flow. All of these systems have stationary walls through which to probe or to inject a tracing fluid into the stream for visual observation.

Harvey (1962) (4) presented the results of an experiment to investigate the swirling flow phenomena. In that experiment he used a clear tube through which air was drawn by a small fan mounted at the downstream end. The swirl was imparted to the air by a set of adjustable vanes mounted in the inlet section. To observe the flow pattern, Harvey used titanium tetrachloride smoke injection and photographed the resulting trace. With this technique he measured the swirl angle, ϕ (ϕ = arctan V_θ/U) distribution. Harvey observed that when the conditions of the incoming flow were such that the swirl angle was large (greater than 50 degrees) the swirling flow contained a region along the centerline where the axial velocity was directed opposite to that of the main flow in the tube. When the swirl angle was less than 50 degrees, Harvey did not observe an axial velocity reversal along the centerline.

Youssef (1966) (5) measured the static pressure and velocity distributions in a rotating flow with a five-port spherical probe. The calibration technique was essentially identical to Bryer's (11) which is described in Section 1.3. The swirl was imparted to the air in the pipe by a set of adjustable vanes at the inlet. The profiles were measured at various downstream locations in the pipe. In this experiment, Youssef observed a reverse flow region near the center of the pipe.

Eckert and Hartnett (6 and 7) conducted experiments inside a 3 inch diameter vortex tube in which air was injected tangentially into the tube at the head end. In these experiments, they used a Kiel probe for the measurement of total pressure and a modified Prandtl probe for measuring the static pressure. The velocity profile was calculated from the measurements of total pressure and total temperature and the static pressure. They found that measurements taken near the centerline (less than 0.5 inches radius) proved to be erratic and not repeatable.

Lay (1956) (8) performed vortex tube experiments similar to those conducted by Eckert and Hartnett using a static pressure probe and a hot-wire anemometer to measure the components of the flow velocity. He also indicated that the results near the centerline were not repeatable. Lay also conducted some flow visualization studies which indicated a reversed flow region. He stated that hypodermic probes are ideally suited for the purpose of taking measurements and hoped that a single multipurpose probe could be designed which could be used for both pressure and velocity measurements.

In summary, previous investigators have observed two types of swirling flows. These are characterized by:

(1) a swirling flow in which the axial velocity of the fluid is moving in one direction;

(2) a swirling flow in which a region of the flow has an axial velocity in a direction opposite to that of the main flow axial velocity.

These two types of swirling flow are more commonly referred to as swirling flows with and without axial velocity reversals.

A second characteristic of a swirling flow, which has been observed by several investigators, is associated with measurements conducted near the centerline. These measurements have proved to be erratic and not reproducible.

Nearly all of the various measurement techniques have been employed for swirling flow measurements. These included flow visualization techniques, hot-wire anemometers and impact tubes. Usually, the measurement technique employed was selected on the basis of the flow quantities to be determined for the particular apparatus and its associated flow field where the measurements were to be conducted.

Before the various measurement techniques could be evaluated, it was necessary to examine the cold-flow apparatus and the flow field for problems that could influence the probe selection.

1.2 A Brief Description of the Cold-Flow Apparatus

Figure 1 illustrates the general arrangement of the spinning, cold-flow rocket motor. A complete description of the apparatus is included in references (3) and (9).

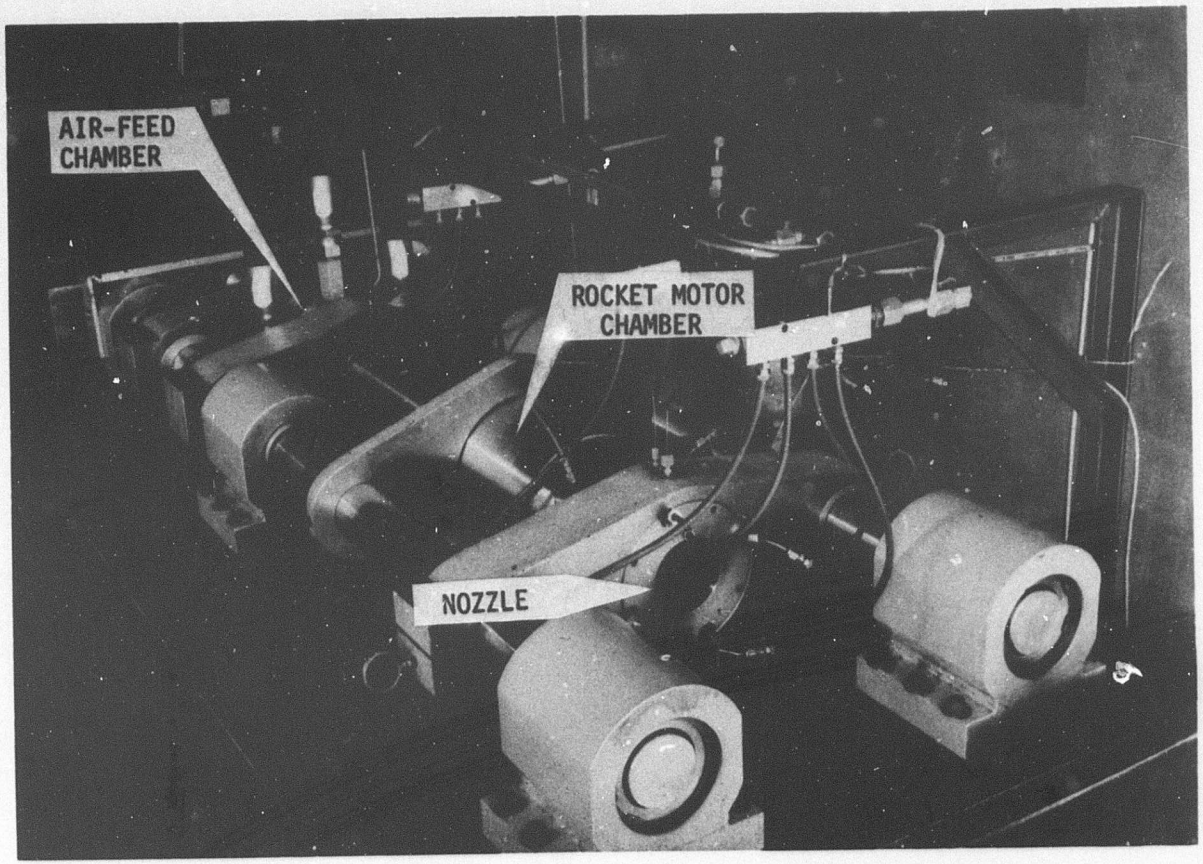

Figure 1 Photograph of the Cold-Flow Spinning Rocket Motor

The apparatus consisted of a stationary air-feed chamber and a rotating rocket motor chamber and nozzle. The rocket motor chamber was connected to the air-feed chamber by means of a hollow drive shaft. The rocket motor was supported horizontally on bearings located at the nozzle and in the air-feed chamber. The rocket motor was rotated about its longitudinal axis by means of an 8-inch Barbour-Stockwell air turbine which was directly connected to the hollow drive shaft. The entire rotating assembly was supported on two rods which were mounted in linear bearings.

Air was supplied to the cold-flow rocket motor from a set of storage tanks at a pressure of 2500 psig. The pressure was reduced to approximately 1000 psig through a regulator. The air flowed through a separator, a filter, an ASME metering orifice, a flow control valve and into the air-feed chamber. The air then flowed through the hollow drive shaft into the head end of the 5.5 inch inside diameter rocket motor chamber.

Upon entering the head end of the rocket motor chamber, the air was passed through a porous surface to simulate the flow emanating from an end-burning grain. The simulated end-burning grain consisted of a sintered steel plate attached to the upstream side of an aluminum plate. The one inch thick aluminum plate channeled the flow through 696 holes of 0.125 inch diameter located symmetrically about the axis of rotation. The sintered steel plate was used to produce a large axial pressure drop which was necessary to minimize the variation of the local mass flow per unit area across the grain surface due to the increasing radial pressure gradient with rotation.

The important feature to note in the photograph of the apparatus is that the entire assembly, including the cylindrical chamber and nozzle, was rotated about the longitudinal axis to impart the swirl to the flow. This is the primary departure from previous experimental studies involving the probing of swirling flows. As mentioned in Section 1.1, previous studies have been confined to vortex tubes and pipe flow, which used adjustable vanes or tangential injection to impart a swirl component to the flow. Those systems have stationary walls to probe through which greatly facilitates probing operations as will be discussed in Section 1.3. The difficulty in the subject cold-flow apparatus is that the only accessible opening through which a probe may be inserted is the nozzle, and the necessity of minimizing the obstruction of the nozzle throat area necessarily limits the size of any apparatus inserted.

The nature of the flow field within the chamber presents a second problem. When the apparatus is rotating the flow field consists of an axial velocity component, a tangential velocity component due to rotation, and, at least near the converging section of the nozzle, a radial velocity component. Thus, the flow field is three-dimensional, imposing further difficulties in the measurements.

The probe system selected for the measurements must, therefore, be small to be inserted through the nozzle and be capable of three-dimensional flow measurements.

1.3 Probe Selection

The first objective of the investigation was to select a suitable probe that could be calibrated for use in the chamber of the

spinning, cold-flow rocket motor. The probe selection was based on the following criteria:

(1) static pressure, velocity magnitude and flow direction must be measured;

(2) as many of these quantities as possible must be measured with one probe, preferably all three;

(3) the probe must be small enough to be capable of point measurement without appreciably affecting the flow by its presence.

Using these criteria, a review of probing techniques was undertaken.

Numerous probing techniques were considered for the velocity and pressure measurements. In general, these could be arranged into the following four distinct groups.

(1) various types of flow visualization and tracing techniques;

(2) hot-wire anemometer;

(3) laser velocimeter;

(4) impact tubes.

The first of the techniques listed, flow visualization and tracing techniques, was ruled unfeasible because of the construction of the cold-flow apparatus. These techniques require that the flow field be visible to a detection system in the region of interest. An additional problem is that these techniques are usually only used in very low speed, laminar flows.

The second technique, hot-wire anemometry, was ruled impractical for this application because of the amount of contaminant in the air supply. Particles would cling to the wire and change the

operating characteristics of the tip. The calibration of the hot-wire would be meaningless and any results highly unreliable.

The laser velocimeter is a new approach in the realm of fluid flow measurements. This system has numerous advantages such as minimal flow disturbance and the capability of working in a three-dimensional flow field. However, at the present time this technique has two significant disadvantages.

(1) a general lack of experience with this technique; this system is still in the research phase and is only being used in controlled experiments where the laser system is the experiment;

(2) the commercial availability of this type of equipment is limited and the units available are very expensive.

Furthermore, the construction of the cold-flow apparatus presents additional problems. The output of the laser would have to be directed through the nozzle and this would require the placement of delicate optical equipment in the air stream. In addition, a back scattering technique would have to be used and this technique requires extremely powerful laser systems and research in this area is only now being explored. For these reasons, a technique other than the laser velocimeter was required. Nevertheless, in a few years, this technique could revolutionize fluid-flow measurements, particularly swirling-flow measurements.

There are many types of impact tube probes ranging from the simplest, the pitot tube, to more complex configurations. In order to use a pitot-static probe in a three-dimensional flow field the

probe must be aligned into the velocity vector. This would require a mechanical system with two degrees of freedom, i.e., rotations in the pitch and yaw planes. This is a difficult scheme even when probing radially through a stationary wall.

All of the probes currently being used for three-dimensional measurements are of the five-port type. The five-port probes are constructed such that two side ports are located in each of two perpendicular directions or planes, pitch and yaw. The central port is used to sense total pressure. The configurations most commonly used are the five finger claw probe, the cobra probe and the spherical probe. These three five-port probes are illustrated in Figure 2.

Winternitz (1956) (10) and Bryer et al. (1955) (11) each presented a comparative survey of different types of impact tube probes for three-dimensional flow measurements. Both articles preferred the cobra head, first suggested by Conrad, because of the close spacing of the tip orifices which simplifies the manufacturing of small probes. Winternitz discussed the conical head where the holes are drilled, whereas Bryer suggested the use of five hypodermic tubes for the probe head which even further simplifies construction of the probe. These reports were concerned primarily with wind tunnel applications where a single degree of freedom alignment was possible. In such a scheme, the five-port probe was rotated, mechanically, in one plane of rotation to null the pressure readings in two of the opposing ports. Calibration charts for the central and remaining side ports were used to determine the remaining flow parameters.

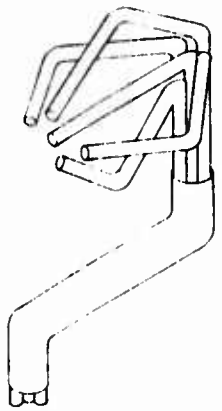

Claw Probe

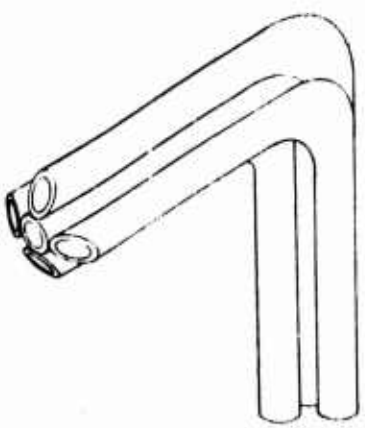

Cobra Probe

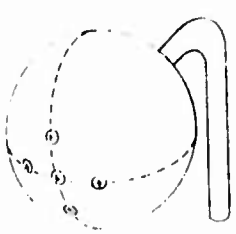

Spherical Probe

Figure 2 Three Five-port Impact Tube Probe Configurations

In the subject cold-flow apparatus, with the probe inserted through the nozzle opening, even a single degree of freedom alignment was considered impractical because of the complexity of constructing a mechanism to rotate the probe and still maintain the structural rigidity of the probe. Therefore, a complete calibration of the five-port impact tube probe was required to enable the pressure and velocity magnitude and direction to be determined from the measurements of the pressures in the five ports. This would eliminate the necessity of rotating the probe within the rocket motor chamber.

Ash and Lee (1956) (12) presented a scheme for calibrating a five-port spherical probe without an adjustment of the probe in the flow field, i.e., a complete probe calibration. They found that the calibration results were highly dependent on the accuracy with which the probe orifices could be located and drilled.

Of the various five-port probes examined, the cobra probe suggested by Bryer et al. (11) was selected for making the measurements in the subject investigation. This probe offered the advantages of being the simplest to construct and duplicate, if necessary. The five finger claw probe is the largest, highly susceptible to damage and would be difficult to duplicate exactly. The spherical probe is difficult to construct accurately. If a duplicate were required, the calibration would have to be repeated.

A description of the probe selected is given in Section 2.1. The complete calibration scheme used was a modification of the method presented by Ash and Lee and is described in APPENDIX A.

2. EXPERIMENTAL APPARATUS

The experimental investigation was divided into two phases: (a) calibration of the five-port impact tube probe and (b) measurements of the velocity and pressure profiles in the radial direction at axial locations near the simulated end-burning grain and the nozzle entrance in the chamber of the spinning, cold-flow rocket motor. The apparatus associated with the calibration phase consisted of the impact tube probe and the calibration tunnel. The only additional apparatus required for measurements in the cold-flow apparatus was the probe traversing mechanism required for making measurements at the two axial locations within the rocket motor chamber. The details of the experimental apparatus are described in this chapter.

2.1 The Impact Tube Probe

The five-port impact tube probe selected in Section 1.3 is illustrated in Figure 3. The probe was constructed from five 304S stainless steel, hypodermic tubes. The outside diameter of the tubing was 0.032 inches and the inside diameter was 0.020 inches. The five hypodermic tubes were bent individually in a jig into the hook shape shown in the photograph and bonded as a unit with an epoxy adhesive. The hook shape was required for the calibration to fix the probe tip location along the radial axis of the probe. Thus, the probe tip

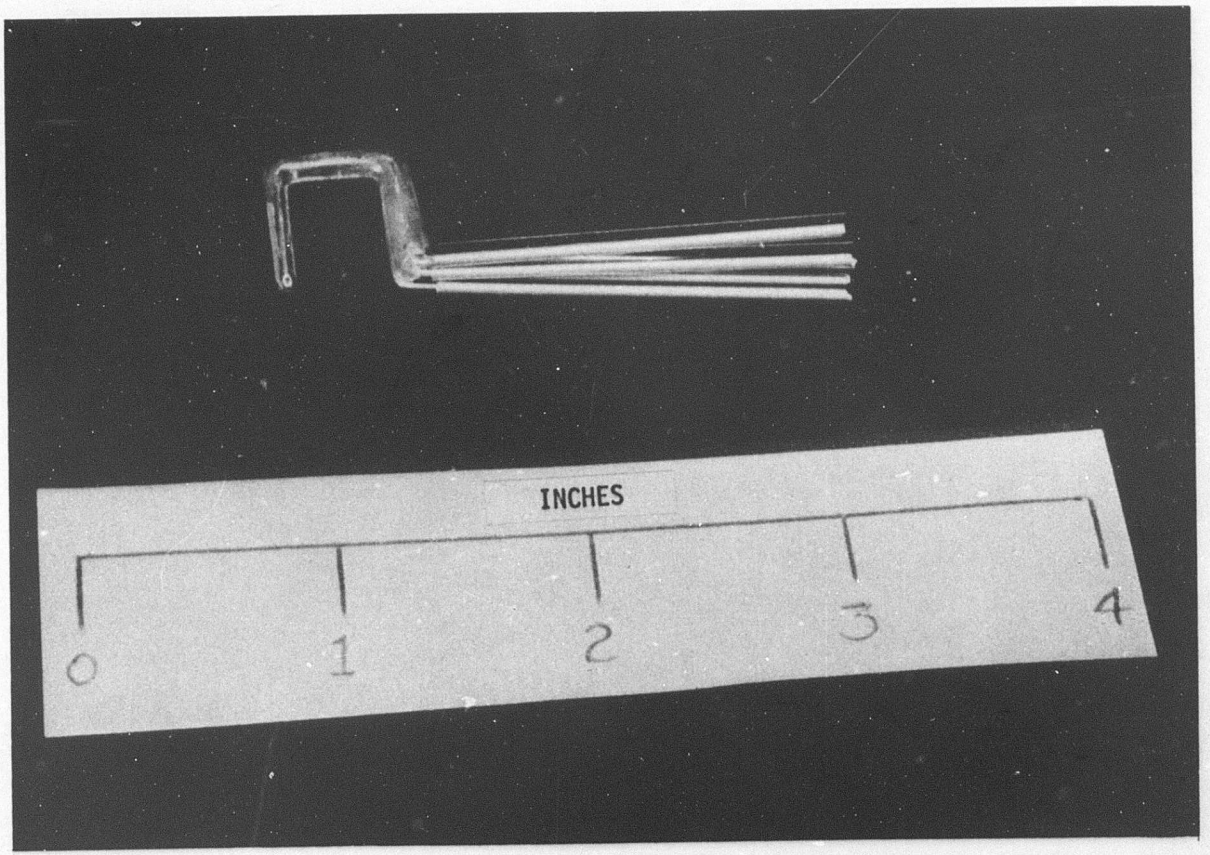

Figure 3 Photograph of the Five-port Impact Tube Probe

location (i.e., point of measurement) did not change as the probe was rotated about the radial axis to vary the orientation of the yaw ports.

The forward ends of the four side tubes were chamfered with a miniature grinder. The apex angle formed was 70 degrees. Details of the probe tip are shown in Figure 4 and are essentially the same as those presented by Bryer et al. (11).

Hyloflow* nylon pressure tubes 0.125 inches outside diameter and 0.078 inches inside diameter were epoxied to each of the five hypodermic tubes. The nylon tubes were then attached to three mercury-filled Meriam U-tube manometers and a Statham 0-1000 psi pressure transducer as illustrated in Figure 5. The manometers were used to measure the differential pressures for each set of ports, i.e., the yaw angle differential pressure (p_2-p_4), the pitch angle differential pressure (p_1-p_3) and the reference differential pressure (p_5-p_1). The pressure transducer was used for measuring the central port pressure, p_5.

2.2 The Calibration Tunnel

The calibration of the probe was conducted in the variable velocity, air tunnel illustrated in Figure 6. The chamber was a Plexiglas** cylinder 2.0 inches long with an inside diameter of 5.94 inches. The nozzle block was fabricated from three sheets of Plexiglas

---

* Trade name of the Polypenco Division of the Polymer Corporation. The manufacturers suggested a maximum working pressure of the nylon tubing of 625 psia.

** Trade name of the Rohm and Haas Company.

D	d/D	Apex Angle
0.032 in.	0.625	70 degrees

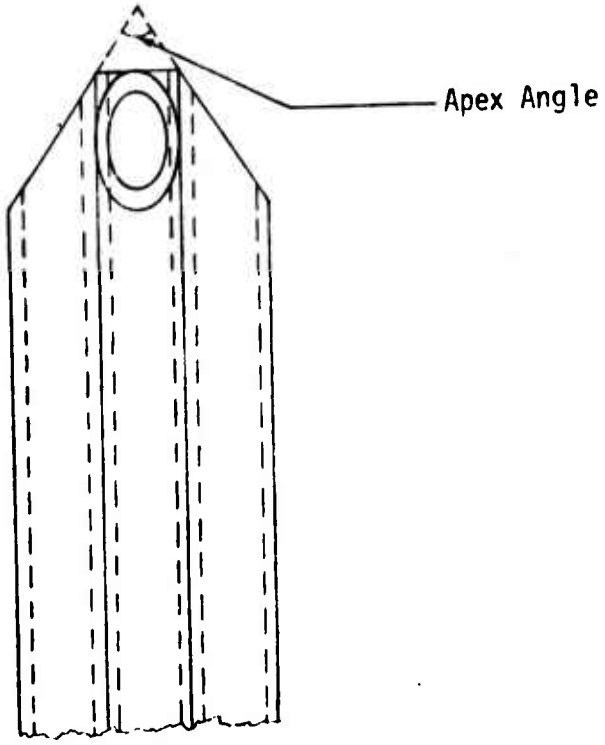

Top and Side View

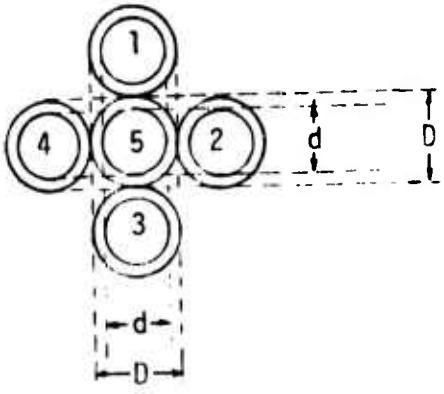

Front View

Figure 4 Details of the Five-port Impact Tube Probe

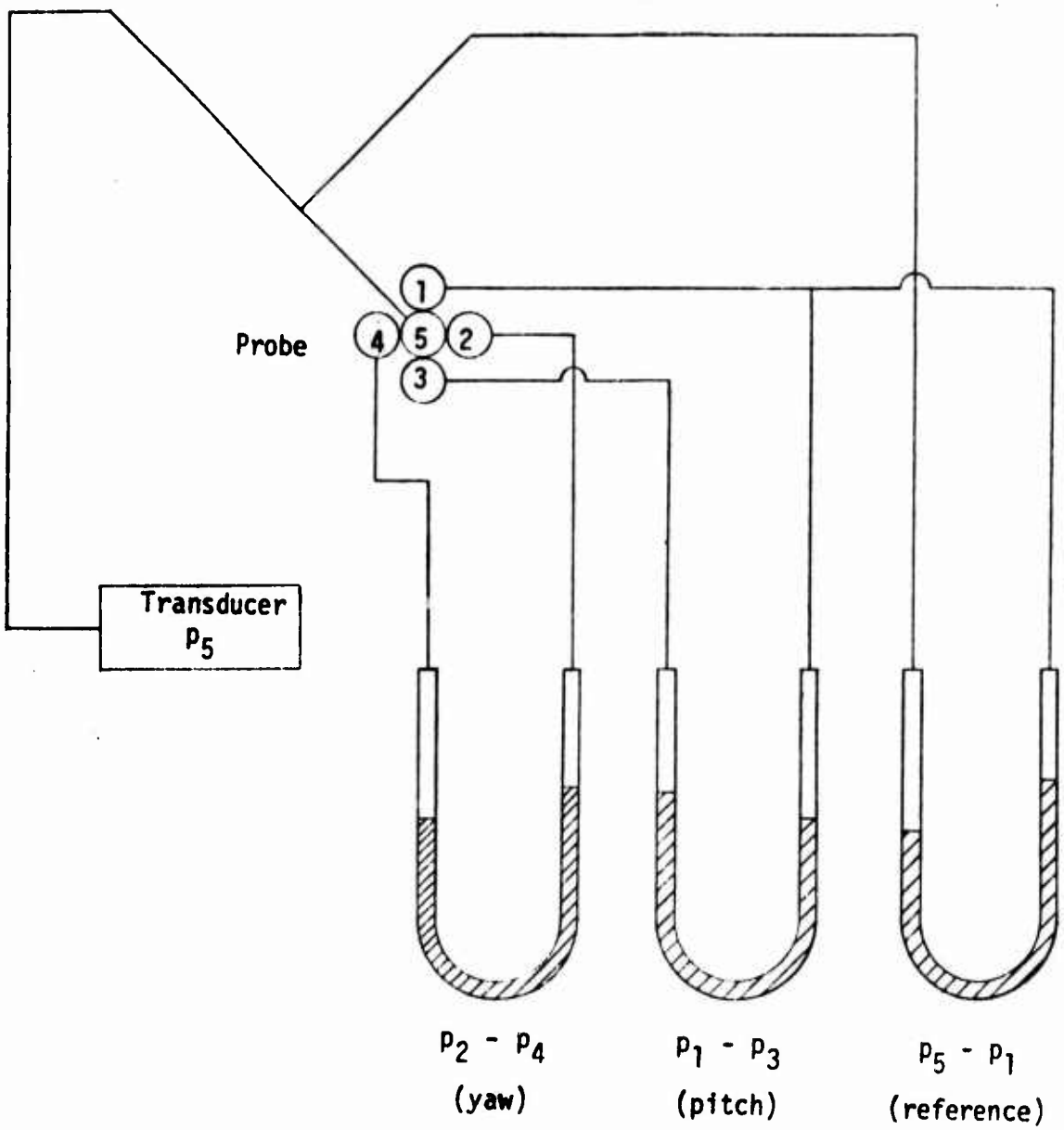

Figure 5 Schematic of the Manometer and Transducer Installation

laminated together to form a total thickness of 4.375 inches. The half angle of the converging section was 45 degrees and the nozzle throat diameter was 1.5 inches.

The head end of the tunnel consisted of an aluminum housing and a 6.5 inch diameter plate with 600 holes for air injection. Air was supplied to the tunnel from a set of storage tanks at a pressure of 1500 psig. The pressure was reduced to 500 psig through a Grove regulator. The air then flowed through an ASME orifice, a flow control valve and into the tunnel housing.

A simple probe mount for the calibration was constructed as shown in Figure 6. The calibration probe mount was constructed to position the probe tip in a plane perpendicular to the nozzle axis approximately 3 inches downstream from the nozzle exit plane. The probe mount allowed the probe tip to be rotated about the X-X axis. The rotation around the X-X axis corresponded to varying the yaw angle, ψ. The orientation of the X-X axis with respect to the nozzle axis was varied in the plane of the test table by rotating the entire probe mount. This last operation was accomplished by pinning the probe mount to the test table directly under the probe tip and rotating the probe mount about this forward pin. The rotation of the X-X axis to the X'-X' axis shown in Figure 7 corresponded to varying the pitch angle, θ. The desired angular position of the probe mount was maintained by positioning a rear pin in any of several holes laid out on the test table. These holes were located at 10 degree increments for a range of pitch angle of ± 30 degrees. The angle of rotation around the X-X axis of the probe was measured with a protractor dial shown in the

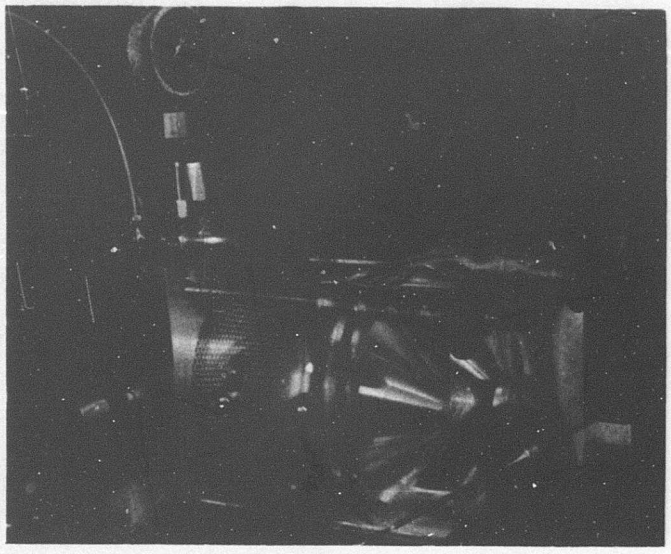

Figure 6 Photograph of the Calibration Tunnel

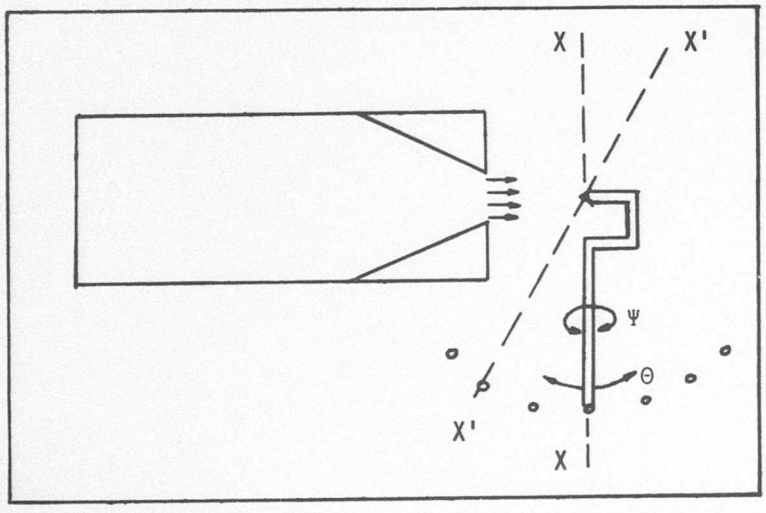

Figure 7 General Arrangement of the Calibration Tunnel and Probe Mount

photograph. Using this technique, the pitch and yaw angle orientation of the probe tip with respect to the calibration tunnel flow could be determined within ± 1 degree.

2.3 The Probe Traversing Mechanism

In order to make measurements of the pressure and velocity profiles at two axial locations within the chamber, a probe traversing mechanism for remote operation was required. Figure 8 presents the general arrangement of the mechanism for traversing the probe inside the chamber of the spinning, cold-flow rocket motor. The traversing mechanism consisted of the following four sub-assemblies:

(1) Outer support tube

(2) Spindle support

(3) Rack and probe

(4) Probe support and motor mount

The outer support tube was constructed from a 27-inch length of 0.25 inch diameter 304S stainless steel tubing with a wall thickness of 0.035 inches. The forward end of the tube was threaded to receive a cap nut which is on the spindle support. The spindle support is a shaft with a cap nut that threads onto the outer support tube and fits through two tandem bearings located in the center of the simulated end-burning grain (drilled aluminum injector plate). The shaft is secured on the back side of the injector plate. This allows the entire chamber and nozzle assembly of the cold-flow apparatus to rotate about the probe.

Five hypodermic tubes to be connected to the probe head were epoxied to an 18-inch length of a small (1/8" x 1/16" cross-section)

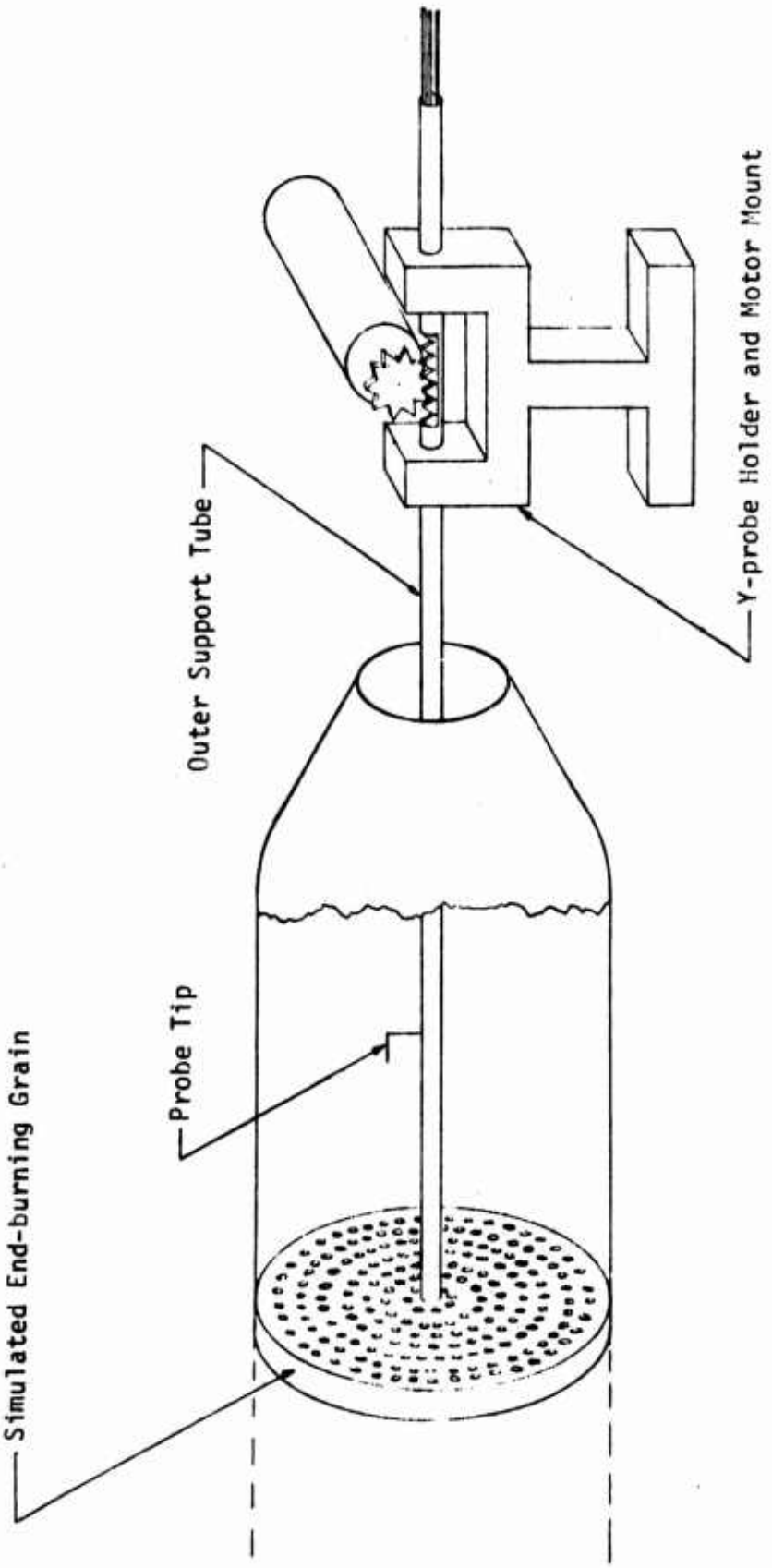

Figure 8 General Arrangement of the Probe Traversing Mechanism

brass rack. This unit, the rack and probe lines, was inserted into the outer support tube. A 0.09-inch wide slot was cut through the wall of the outer support tube for a length of 8 inches, the approximate length of the chamber. The probe lines were bent and protruded through the slot on the outer support tube. This type of installation allowed the probe head to be attached to the five lines protruding from the outer support tube. The attachment was accomplished by using short lengths of hypodermic tubing for sleeves. The sleeves were epoxied to the lines protruding from the outer support tube slot and the probe head.

A Y-probe holder and motor mount was located downstream of the nozzle of the cold-flow apparatus and secured to the test stand. The outer support tube was secured to the Y-probe holder and a low speed servo motor was used to drive the rack and probe unit in the axial direction. The longitudinal speed of the probe was approximately 3 inches per minute. The probe traversing mechanism is shown in Figure 9 with outer support tube in place in the cold-flow apparatus.

The radial position of the probe had to be changed manually. This required a change in the length of the sleeves that attached the probe head to the probe lines. Sleeves were made in 0.25 inch increments so that the radial position could be changed from 2.5 inches down to 0.75 inches in radius.

For measurements inside the chamber of the rocket motor, it was also necessary to orient the probe tip at an angle to the motor axis of rotation. The angular orientation was established at the same time as the radial position of the probe. This is discussed in greater detail in Section 4.1.

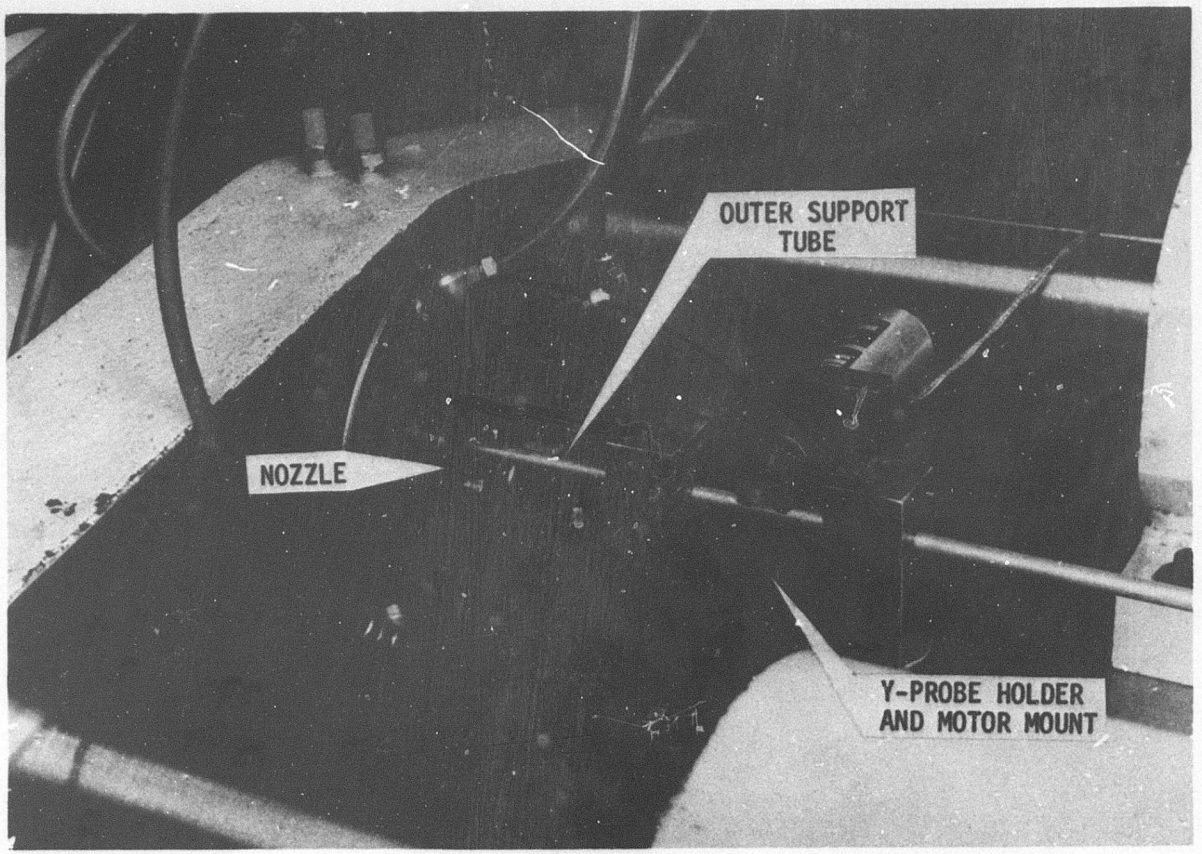

Figure 9 Photograph of the Probe in Place in the Cold-Flow Apparatus

3. CALIBRATION OF THE PROBE

The primary objective of the calibration phase was to obtain charts for determining the static pressure, the velocity magnitude and direction in the chamber of the spinning, cold-flow rocket motor from the measurements of the pressures in the five ports of the impact tube probe. The calibration procedure and the results of the impact tube probe calibration are presented in this chapter. The calibration scheme is presented in detail in APPENDIX A.

3.1 Calibration Procedure

Prior to performing the calibration of the impact tube probe, it was necessary to ensure that the flow in the free jet exiting from the calibration tunnel was of a uniform nature over an area of sufficient size for calibration of the five-port probe. The probe tip was approximately a tenth of an inch in diameter, therefore, to ensure that no velocity gradients were acting on the probe tip the flow would have to be uniform in a region larger than the probe tip diameter. Tests were conducted using a United Sensor pitot-static probe to determine the velocity profile in the free jet. Figure 10 presents velocity profiles taken 3 inches from the nozzle exit plane. This corresponded to the location of the probe for calibration. The data are for nominal free stream velocities of 180 and 300 feet per

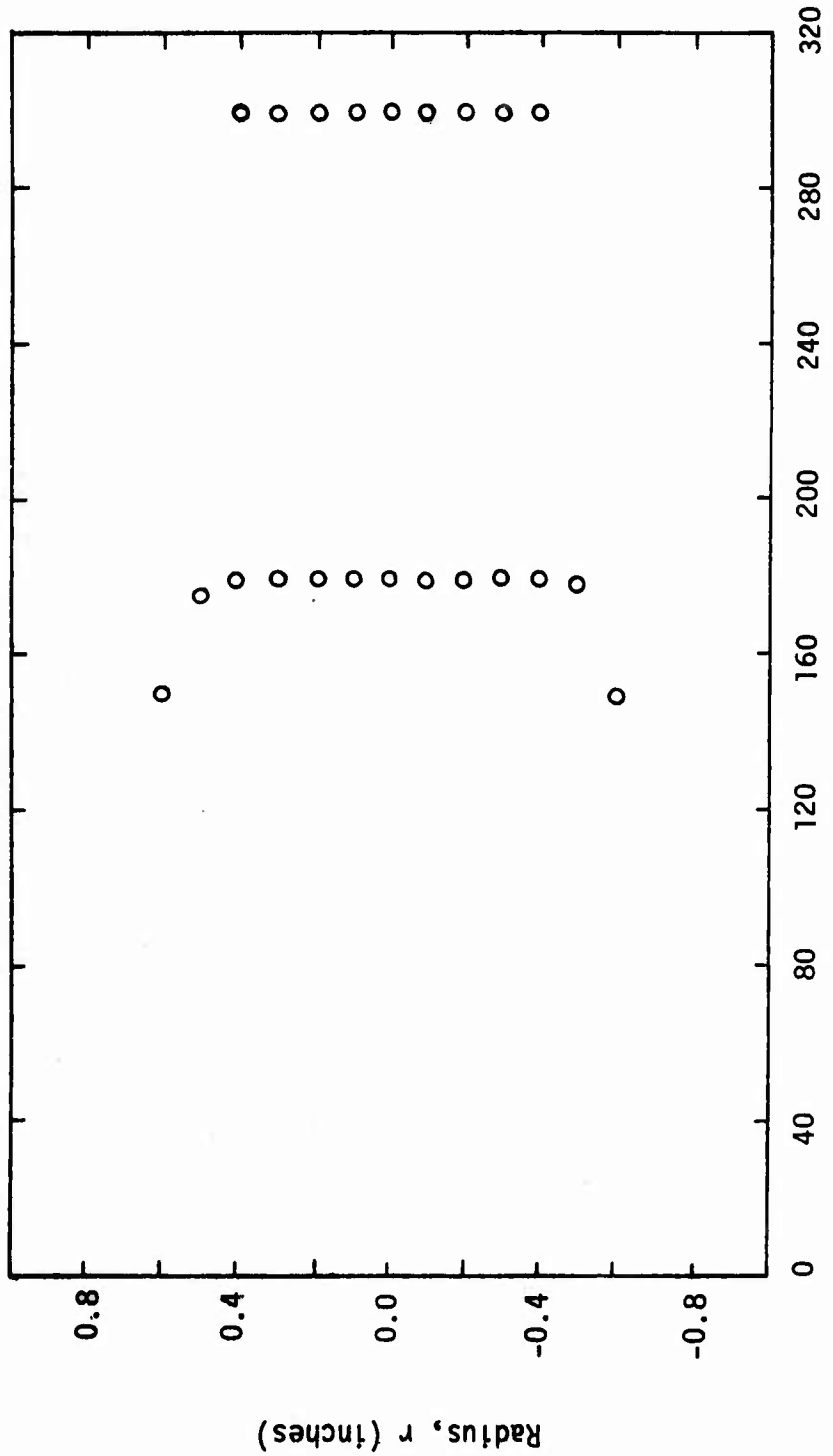

Figure 10 Velocity Profiles in the Calibration Tunnel

second. The profiles were uniform over the central 1.0 inch indicating that velocity gradients at the probe tip could be neglected.

The procedure for the probe calibration was as follows:

1. Obtain steady state flow in the calibration tunnel.
2. Record the chamber static pressure and static temperature.
3. Using the United Sensor pitot-static probe in the test region, record the dynamic pressure. These data were then used to compute the test region velocity.
4. Insert the probe to be calibrated in the test region at 0 degrees pitch and yaw.
5. Record the differential pressure readings for each set of ports, i.e., p_1-p_3, p_2-p_4, p_5-p_1 and p_5-p_{atm}.
6. Vary the yaw angle through a ± 50 degree range in increments of 10 degrees and record the readings listed in step 5.
7. Upon completing step 6 for the complete range of yaw angles, the pitch angle was varied through a ± 20 degree range in increments of 10 degrees and step 6 repeated for each value of the pitch angle.
8. To determine the effect of the test region velocity, the entire procedure was repeated three times for test region velocities of 100, 200 and 300 feet per second.

In all cases the calibration tunnel performed adequately. However, it was found that the tunnel operated more satisfactorily if the outside ambient temperature was above 65 degrees Fahrenheit. At temperatures below this value, ice formed in the pressure regulator

causing the mass flow rate to oscillate, producing an unsteady flow rate. Consequently all tests were conducted when the outside ambient temperature was above 65 degrees Fahrenheit.

3.2 Results of the Probe Calibration

The five-port impact tube probe was calibrated in the calibration tunnel described in Section 2.2 using the scheme discussed in APPENDIX A. The results of the calibration are shown in Figures 11 through 19. Three sets of charts were required for the complete calibration. These were as follows:

1. The flow angle calibration charts presented in Figures 11, 12 and 13.
2. The dynamic pressure calibration charts presented in Figures 14, 15 and 16.
3. The total pressure calibration charts presented in Figures 17, 18 and 19.

Figures 11, 12 and 13 present the flow angle calibration data for test section velocities of 100, 200 and 300 feet per second respectively. The ordinate of each of these charts presents the ratio of the yaw angle differential pressure and a reference differential pressure (p_2-p_4/p_5-p_1 or p_2-p_4/p_5-p_3 depending on the sign of the pitch angle). The change in the reference differential pressure was required to make the curves symmetrical about the ordinate. The abscissa presents the ratio of the pitch angle differential pressure and the same reference differential pressure. Along the ordinate, the zero degree pitch angle curve, p_1 and p_3 are identical and either

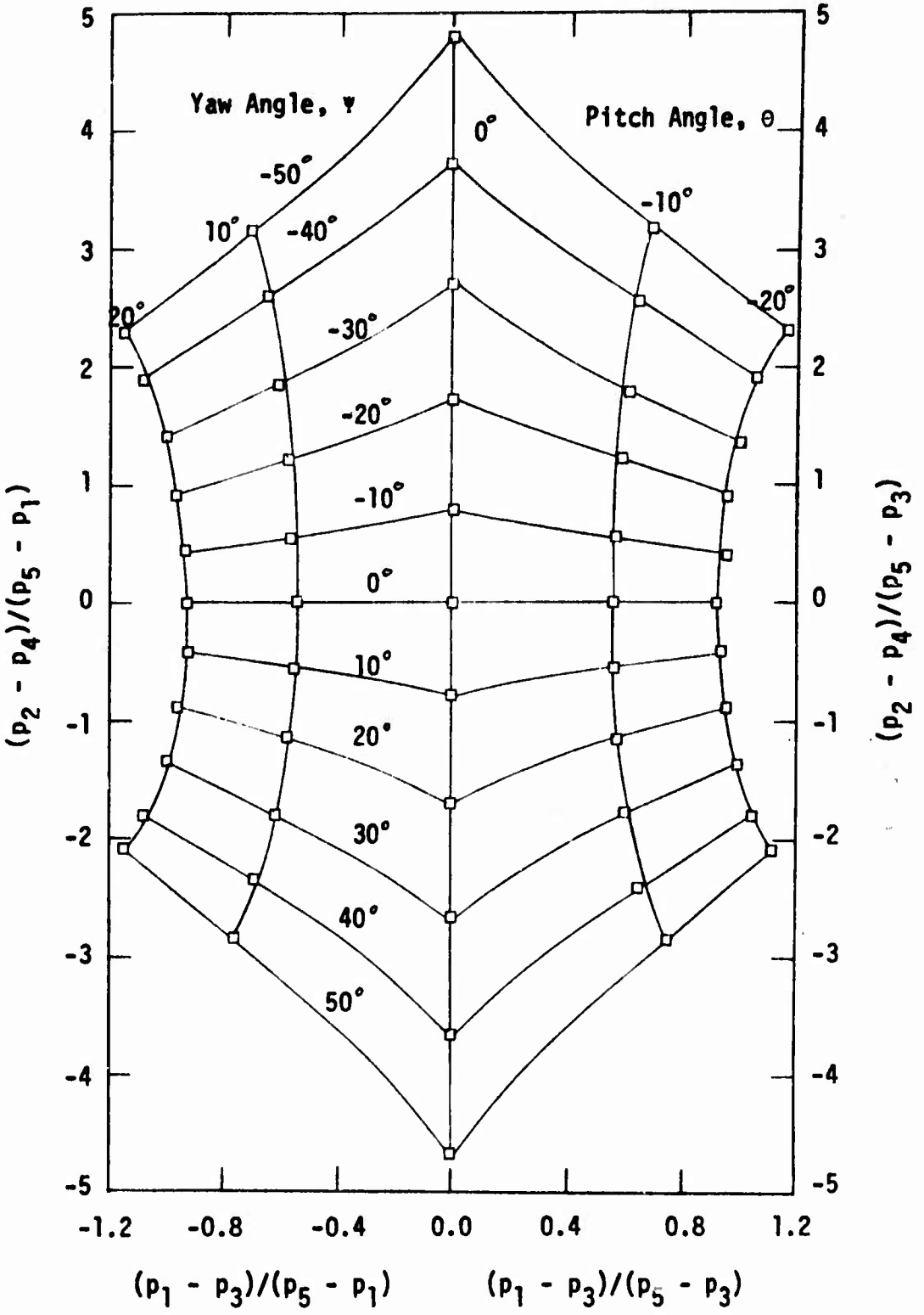

Figure 11 Flow Angle Calibration
Velocity, V = 100 ft/sec

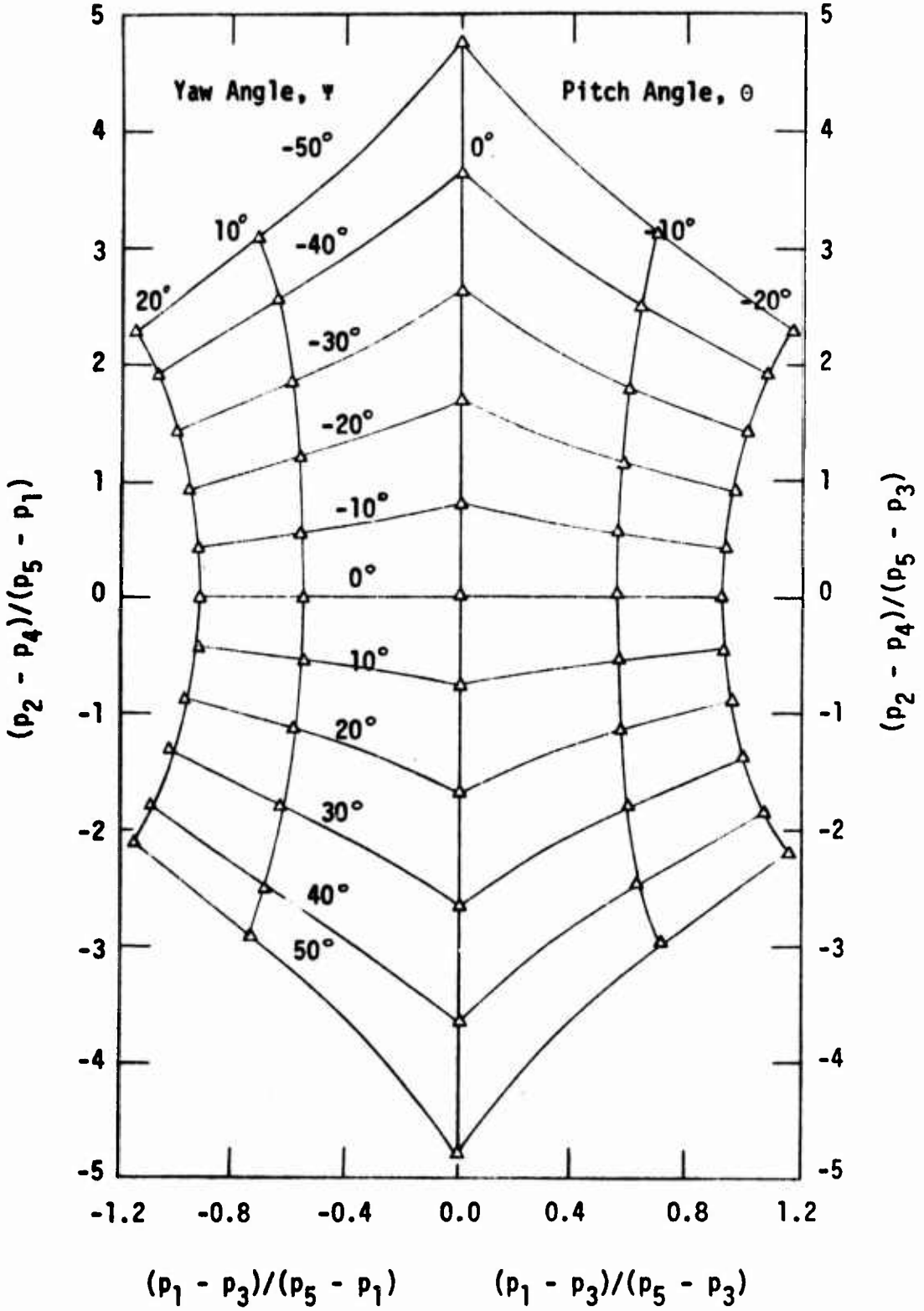

Figure 12 Flow Angle Calibration
Velocity, V = 200 ft/sec

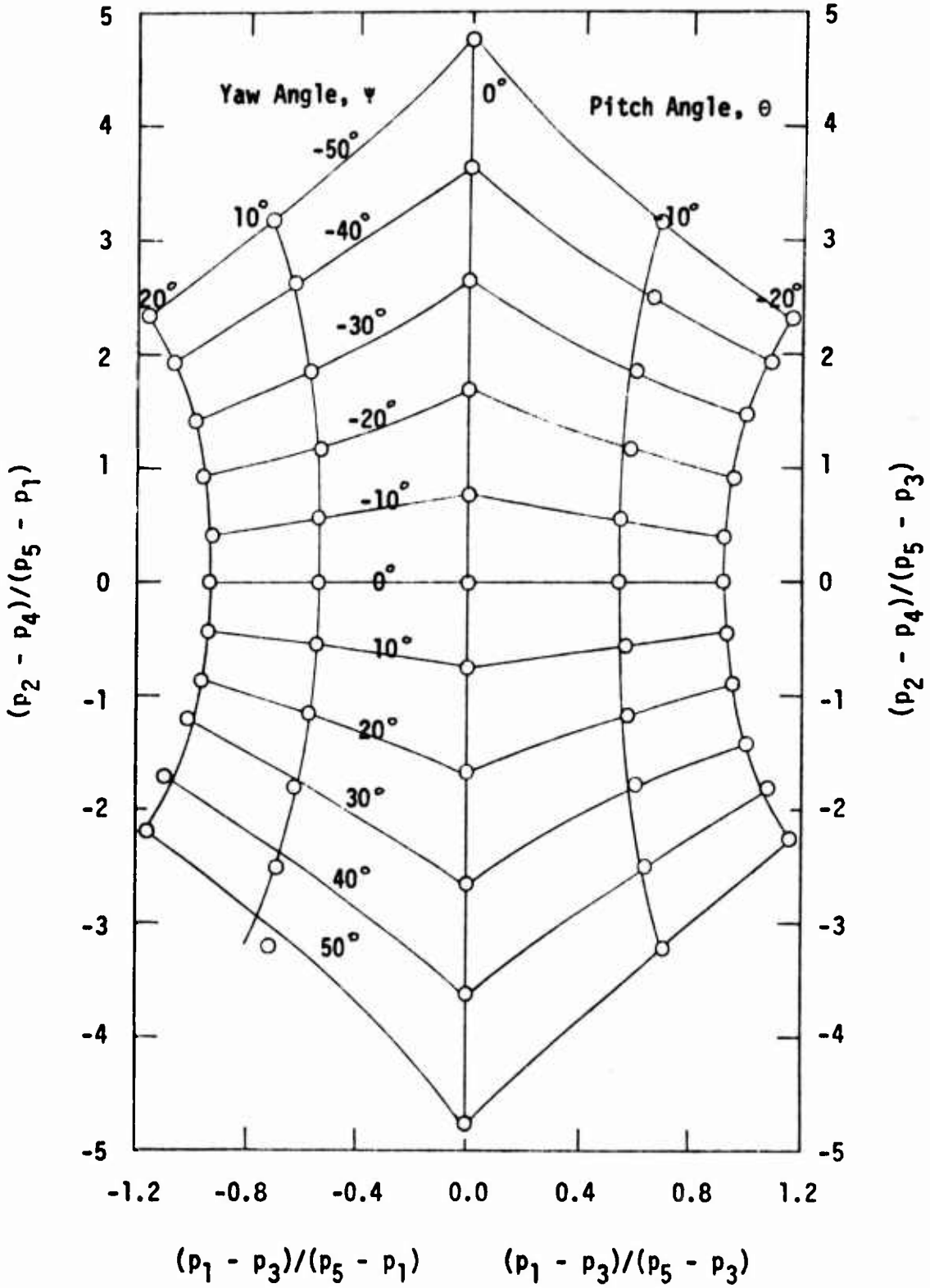

Figure 13 Flow Angle Calibration
Velocity, V = 300 ft/sec

reference differential pressure can be used. Curves of constant yaw angle are shown for a range of ± 50 degrees and curves of constant pitch angles are shown for a range of ± 20 degrees.

Figures 14, 15 and 16 present the dynamic pressure calibration data for a 0 degree pitch angle, ± 10 degrees and ± 20 degrees pitch angle, respectively. The ordinate presents the ratio of the yaw angle differential pressure and the dynamic pressure ($\frac{1}{2}\rho V^2$). Each figure includes data for test section velocities of 100, 200 and 300 feet per second.

Figures 17, 18 and 19 present the total pressure calibration data for a 0 degree pitch angle, ± 10 degrees and ± 20 degrees pitch angle, respectively. The ordinate presents the ratio of the total pressure less the central port pressure and the dynamic pressure. The yaw angle is shown on the abscissa. Each figure includes data for test section velocities of 100, 200 and 300 feet per second.

3.3 Discussion of the Calibration Results

Figures 20, 21 and 22 present composite figures for the flow angle calibration, the dynamic pressure calibration and the total pressure calibration data, respectively. These curves were plotted using the average value of the data points for 100, 200 and 300 feet per second. In general, they closely approximate the 200 feet per second data. The intent was to construct a set of general curves for finding "first values" for θ, ψ, q, H, p and V and then, if necessary, iterate for more accurate results using Figures 11 through 19.

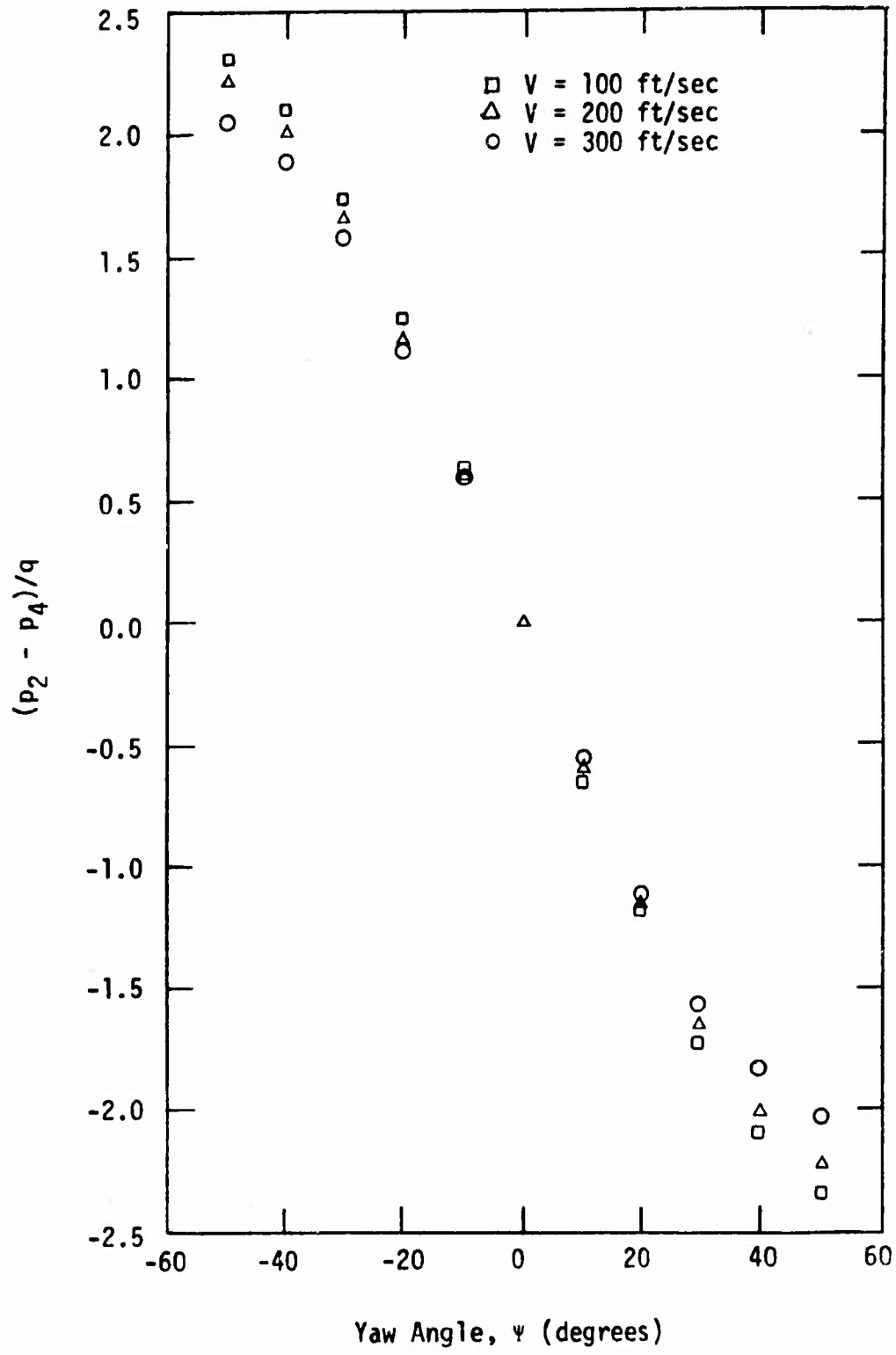

Figure 14 Dynamic Pressure Calibration
Pitch Angle, θ = 0 degrees

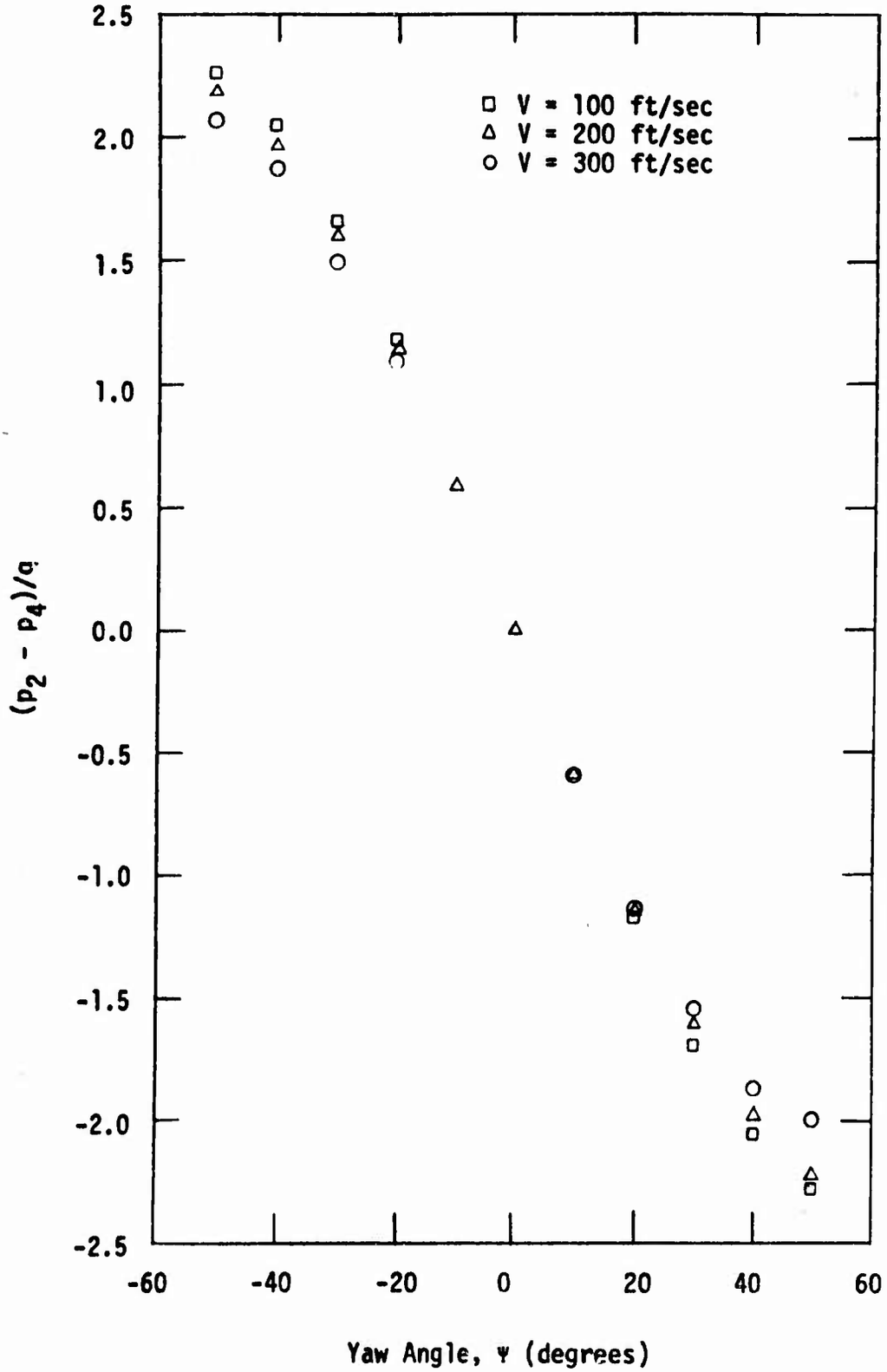

Figure 15 Dynamic Pressure Calibration
Pitch Angle, θ = ±10 degrees

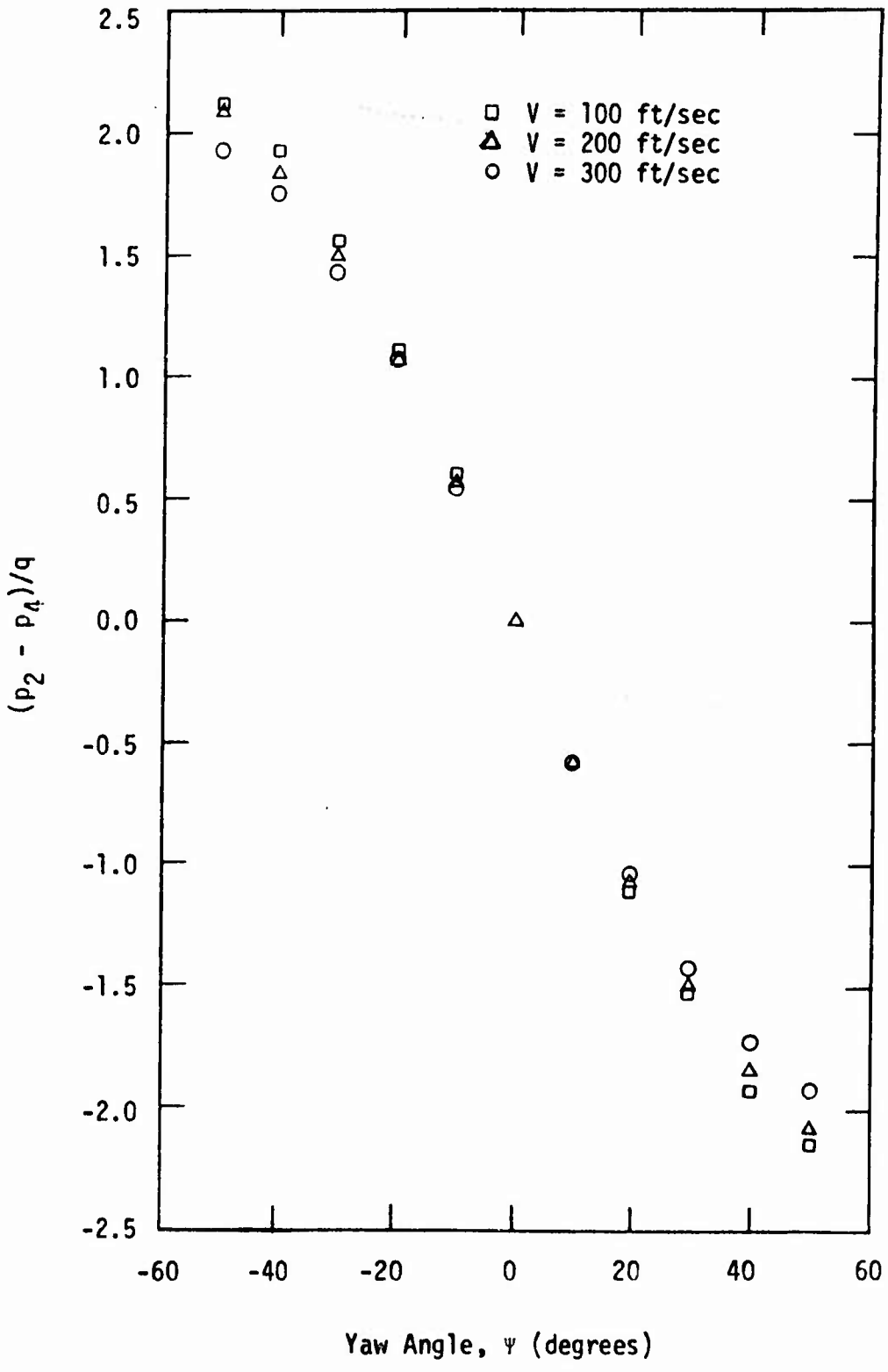

Figure 16 Dynamic Pressure Calibration
Pitch Angle, θ = ±20 degrees

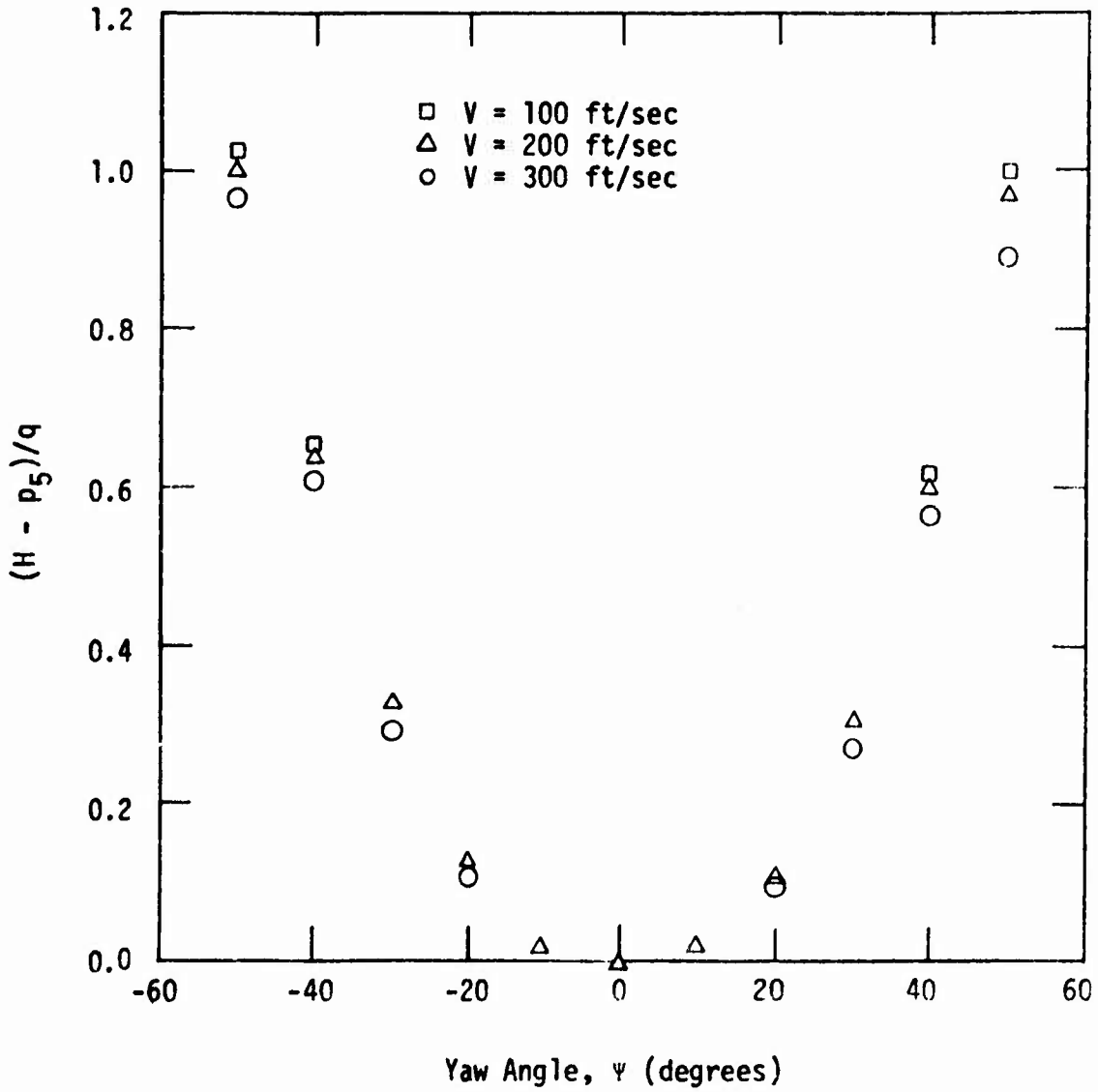

Figure 17 Total Pressure Calibration
Pitch Angle, θ = 0 degrees

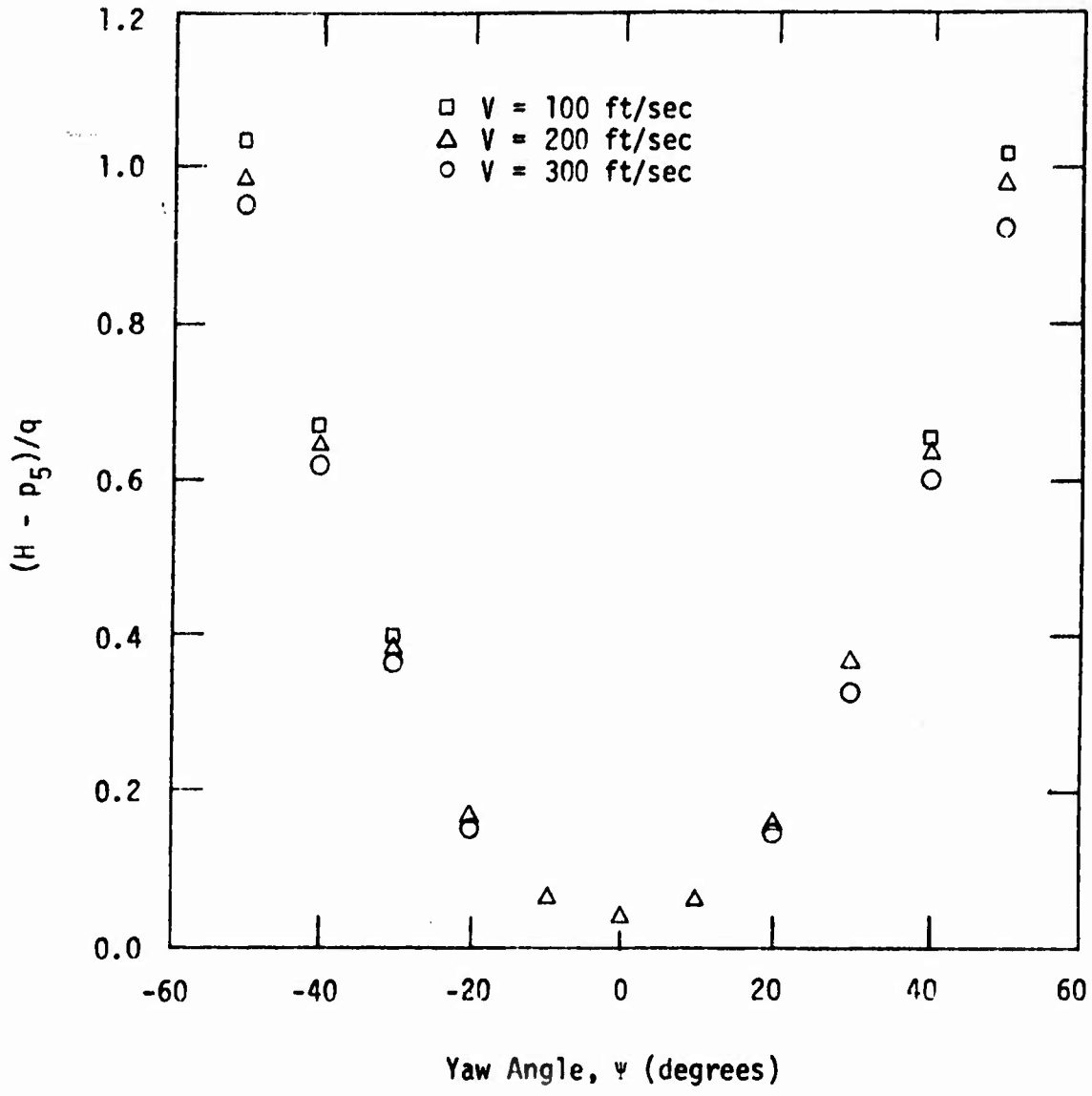

Figure 18 Total Pressure Calibration
Pitch Angle, Θ = ±10 degrees

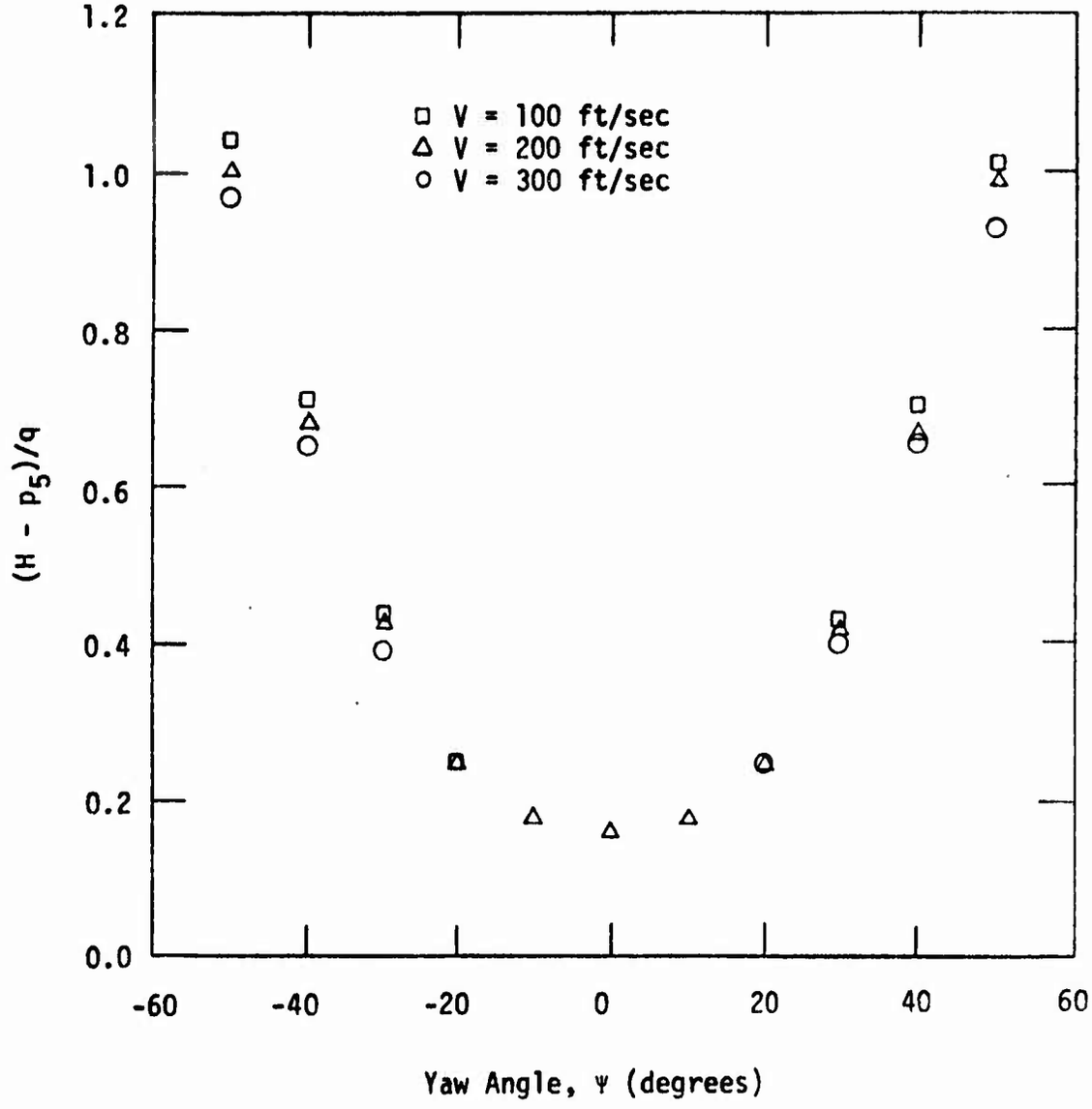

Figure 19 Total Pressure Calibration
Pitch Angle, θ = ±20 degrees

The procedure for using the calibration charts is outlined in the following steps:

1. The manometer readings p_1-p_3, p_2-p_4 and p_5-p_1 are combined to obtain the ratios $(p_1-p_3)/(p_5-p_1)$ and $(p_2-p_4)/(p_5-p_1)$ or $(p_1-p_3)/(p_5-p_3)$ and $(p_2-p_4)/(p_5-p_3)$ depending on the sign of p_1-p_3.
2. Enter Figure 20 and read the pitch angle (θ) and the yaw angle (ψ).
3. Enter Figure 21 with the values of θ and ψ obtained in step 2 and read $(p_2-p_4)/q$.
4. Since p_2-p_4 is known, calculate the dynamic pressure, q.
5. Enter Figure 22 with the values for θ and ψ obtained in step 2 and read $(H-p_5)/q$.
6. Since p_5 as measured by the transducer and q was calculated in step 4, the total pressure (H) can be calculated.

A complete set of sample calculations are included in APPENDIX B.

The use of Figure 21, the dynamic pressure calibration, presents a problem when the yaw angle is nearly zero degrees. The dynamic pressure cannot be determined from the chart. For this case it was necessary to change the orientation of the probe and repeat the measurements so that the yaw angle would have a value other than zero degrees.

The accuracy with which the charts could be used was checked by positioning the probe at some unknown orientation with respect to the air stream in the calibration tunnel, making the appropriate measurements and then determining the flow parameters from the calibration

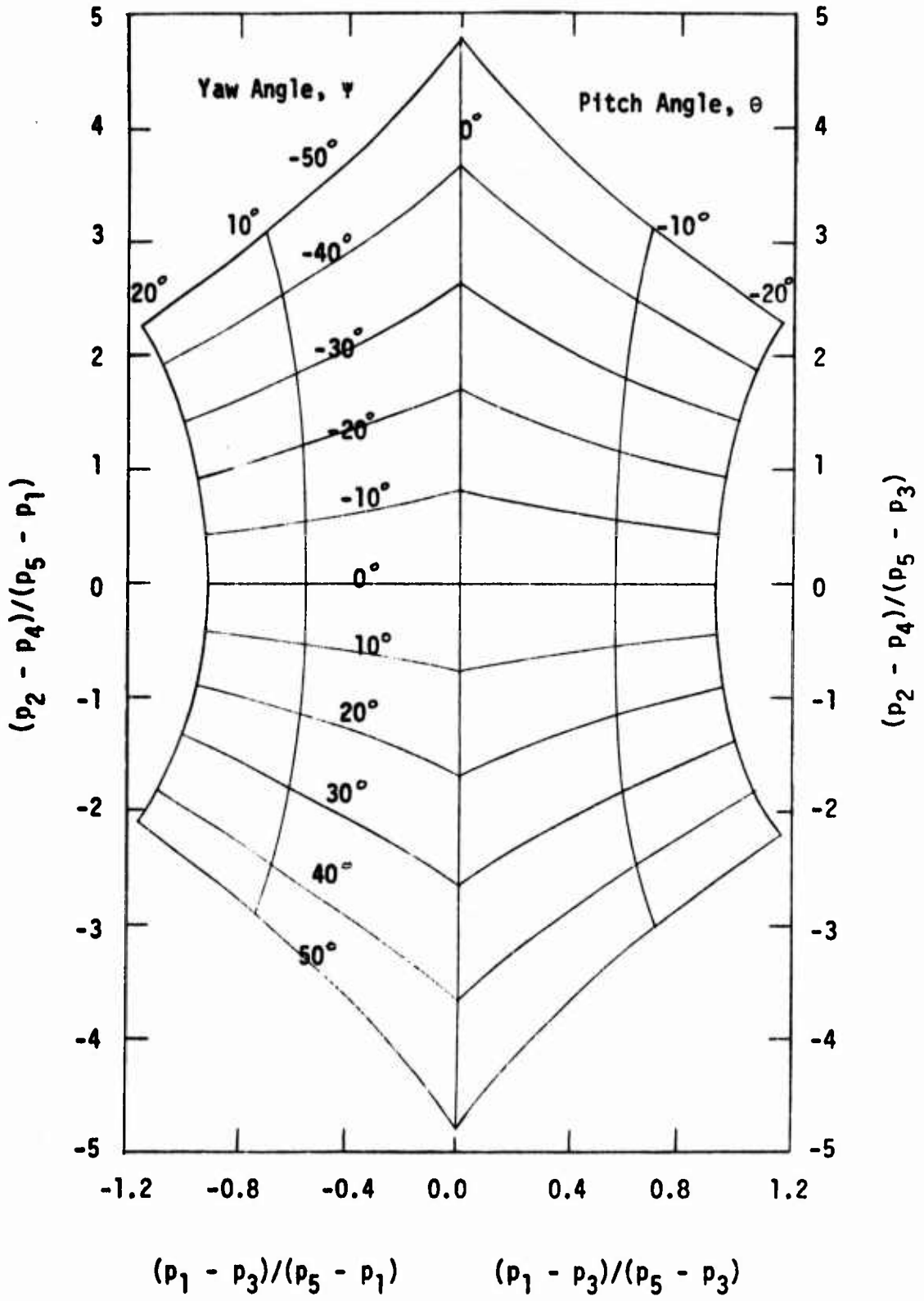

Figure 20 Flow Angle Calibration

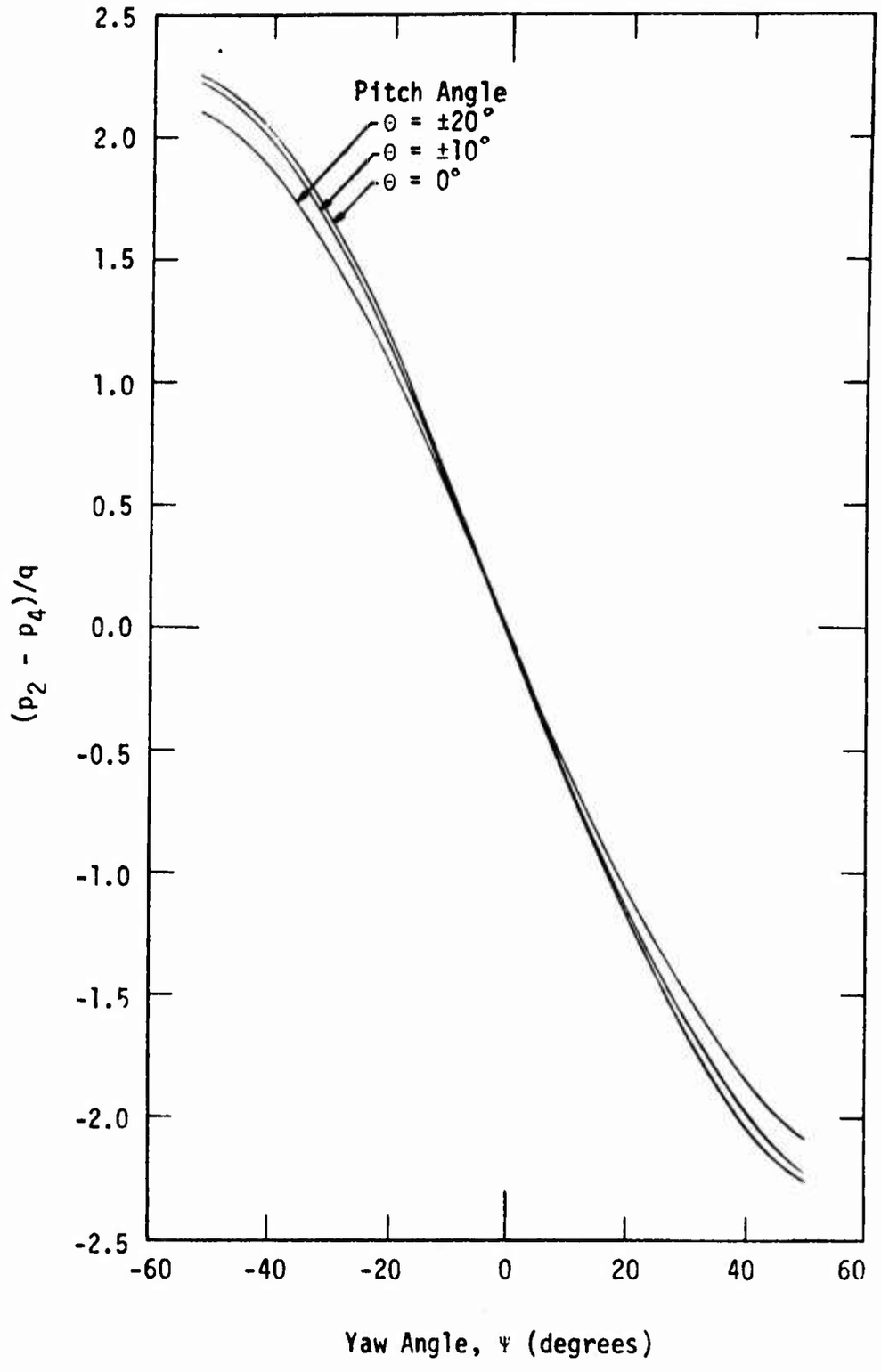

Figure 21 Dynamic Pressure Calibration

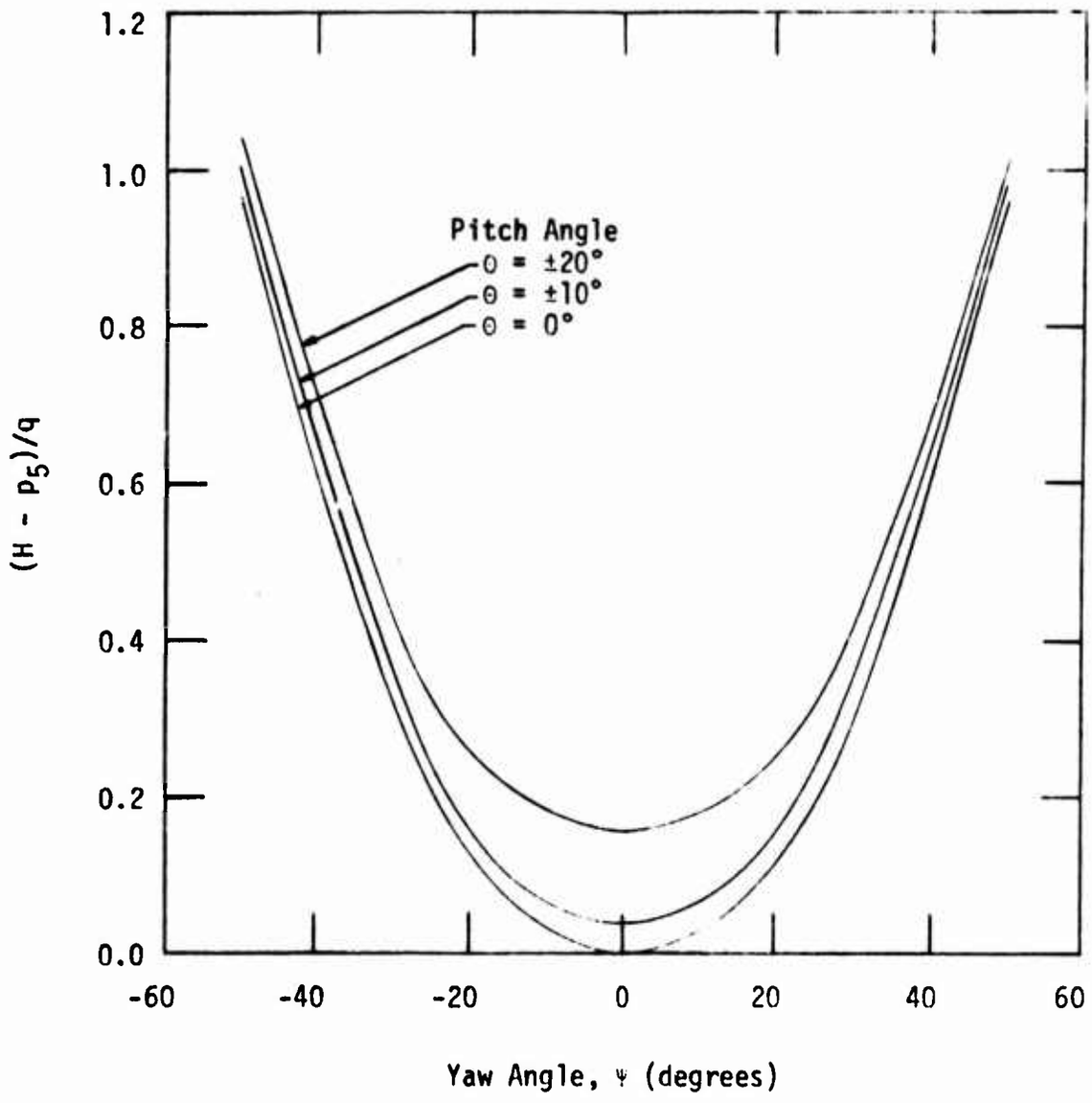

Figure 22 Total Pressure Calibration

charts. The values for the flow velocity magnitude and direction were compared with the actual probe orientation and the air stream velocity and in all cases it was found that the flow angles could be determined within ± 2 degrees. The accuracy for the velocity and static pressure was found to be within ± 5 percent.

The five-port hypodermic probe was selected for its ease of construction. The critical parameters in the construction were the location of the four side tubes and the accuracy of the apex angle formed. If the probe construction is accurately maintained, newly constructed probes should have similar calibration parameters and it should only be necessary to spot check the calibration results. A second probe tip was constructed during the investigation and the spot check revealed identical results within the accuracy of the experimental measurements.

The calibration resulted in a probe capable of determining the static pressure and the magnitude and direction of the velocity vector in a three-dimensional flow without an adjustment of the probe in the flow field when the velocity vector was within the calibration range of the probe. Although some knowledge of the flow field was required, this technique offered a significant simplification when probing in the cold-flow apparatus. Calibrations of this kind are laborious but once completed the time required to obtain results is reasonable.

4. PRESSURE AND VELOCITY MEASUREMENTS IN THE COLD-FLOW APPARATUS

The main objective of the investigation was to determine the pressure and velocity profiles inside the chamber of the spinning, cold-flow rocket motor using the five-port impact tube probe described in Chapter 3. Selection of the experimental conditions, the experimental procedure and the results of probing the flow field are presented in this chapter.

4.1 Selection of Experimental Conditions

Prior to performing the actual pressure and velocity measurements in the chamber of the cold-flow apparatus, it was necessary to select a set of operating conditions for the investigation. The cold-flow apparatus described in Section 1.2 was designed for a broad range of operating conditions. These were:

(1) rotational velocities from 0 to 25000 rpm;

(2) nozzle throat sizes from 0.25 inches to 2.0 inches in diameter;

(3) and chamber pressures up to 800 psig.

Preliminary spin tests were conducted in the cold-flow apparatus with only the outer support tube of the traversing mechanism present. In those tests, the outer support tube failed repeatedly at a rotational speed of approximately 8000 rpm apparently due to the

excessive flexure of the tube due to vibrations. Consequently, all probe measurements were conducted at rotational speeds below this value. In particular, rotational speeds of 1000, 3000 and 5000 rpm were selected as the nominal values for the probe measurements.

The nozzle configuration selected for the principal portion of the investigation was a converging nozzle with a 1.125 inch throat diameter. The selection of this nozzle was based primarily upon the magnitude of the axial velocity component in the rocket motor chamber required to enable an accurate resolution of the flow direction. The one-dimensional axial velocity component in the chamber with the 1.125 inch nozzle was approximately 25 feet per second. The tangential velocity component at 5000 rpm near the motor chamber wall was approximately 120 feet per second. This condition corresponds to a swirl angle of 77 degrees. Thus, a 2 degree error in determining the swirl angle (the accuracy of the calibration charts) could result in a 15 per cent error in the magnitude of the axial velocity component. Smaller throat diameters (i.e., larger nozzle area contraction ratios) reduced the axial velocity component in the chamber which increased the error in determining the axial velocity. With a 0.875 inch diameter throat, for example, a 2 degree error in swirl angle near the chamber wall could result in a 100 per cent error in the axial velocity component.

A brief investigation was conducted using the largest nozzle available, the 2.0 inch diameter throat. The axial velocity component in the chamber for this nozzle was 85 feet per second and a 2 degree error in swirl angle near the wall at 5000 rpm could result

in only a 4 per cent error in the magnitude of the axial velocity component.

An upstream orifice pressure of 400 psig was selected for the investigation because low pressures (below 250 psig) resulted in oscillations of the flow control valve and high pressures (above 600 psig) caused leakage through the shaft seals in the air-feed chamber. An upstream orifice pressure of 400 psig resulted in a rocket motor chamber pressure of 100 psig with the 1.125 inch nozzle and 30 psig with the 2.0 inch nozzle.

Two longitudinal locations were selected for the pressure and velocity measurements. The first location was 2.0 inches downstream of the simulated end-burning grain (injector plate). The probe could not be positioned closer to the injector plate because of the construction of the traversing mechanism. This restriction was required to facilitate removal of the probe from the chamber. The second location selected was at the nozzle inlet, 6 inches downstream from the injector plate. To probe within the nozzle where the velocities were greater than 300 feet per second would have required a much more extensive velocity calibration for the probe. Consequently, probing was limited to the two axial locations within the chamber.

The yaw angle calibration was limited to a range of ± 50 degrees about the velocity vector. This limitation required an initial estimate of the flow angle to be measured to ensure that the probe was positioned such that the velocity vector was included within the calibration range. The initial angle estimate was based on the swirl angle range which was calculated from the assumption of a

one-dimensional uniform axial velocity component and a solid body tangential velocity component for each rotational speed at the radius to be probed. The estimated swirl angle, for a given radial position, varied with the rotational speed in accordance with the variation of the tangential velocity component. Since it was desired to obtain, in a given run, data for all rotational speeds for a particular radial location, the probe was positioned approximately in the center of the calculated swirl angle range for rotational speeds from 1000 to 5000 rpm.

4.2 Experimental Procedure

The procedure for preparing the apparatus for an experiment was as follows:

1. The probe tip was attached to the lines in the traversing mechanism. The radial position and the angular orientation of the probe tip were established for the run at this time.
2. The complete probe assembly was water tested for leaks. This was accomplished by submerging the entire probe assembly in water and blowing air through the lines at a pressure level comparable to the experimental value.
3. The probe was inserted into the cold-flow apparatus and the nylon tubing was attached to the manometers and the pressure transducer. The probe tip was positioned two inches downstream of the injector plate, the closest position the traversing mechanism allowed.
4. Before the run was started the spin rig was allowed to slowly accelerate to approximately 2000 rpm to permit a

gradual warm-up to eliminate any vibrations associated with residual oil deposits on the bearings from the previous run.

Upon completion of these steps, an experimental run was conducted. The procedure that was followed during the course of an experimental run is detailed in the following steps:

1. The spin rig was slowed to 500 rpm and the air was slowly fed to the motor until the flow control valve was fully open.
2. The rotational speed was increased to 1000 rpm and allowed to reach a steady operating condition. At this time the manometer readings, the transducer output and the air temperature were recorded.
3. Upon completing Step 2, the spin rig was increased to 3000 rpm and the data indicated in Step 2 were recorded; similarly, these data were recorded at 5000 rpm.
4. The probe was traversed downstream to the entrance of the converging nozzle and Step 2 was repeated at 5000, 3000 and 1000 rpm.
5. The apparatus was shut down and the entire probe assembly removed in order to change the radial position of the probe tip.

In order to obtain a complete pressure and velocity profile in the radial direction, the entire procedure was repeated for a range of radial positions from 0.75 inches to 2.5 inches in increments of approximately 0.25 inch.

4.3 Experimental Results

The results of the experimental investigation with the five-port impact tube probe inserted in the cold-flow apparatus are shown in Figures 23 through 33. The first data presented were obtained employing the 1.125 inch throat nozzle. The axial velocity component, tangential velocity component and the swirl angle measured at the plane nearest the simulated end-burning grain are plotted versus radius in Figures 23, 24, 25 and 26 for rotational speeds of 1000, 2000, 3000 and 5000 rpm, respectively. Similar profiles measured at the nozzle inlet for rotational speeds of 1000, 3000 and 5000 rpm are presented in Figures 27, 28 and 29.

The axial velocity, tangential velocity and swirl angle profiles obtained by probing in the chamber when the 2.0 inch nozzle was employed are presented in Figures 30, 31 and 32 for rotational speeds of 1000, 3000 and 5000 rpm, respectively. These data are for the probe positioned at the plane nearest the simulated end-burning grain.

The solid lines included on Figures 23 through 32 as references for the data points represent the corresponding profile for a uniform axial velocity and a solid body tangential velocity calculated for the known values of mass flow and rotational speed. The uniform axial velocity distribution was based on the air mass flow rate calculated from the orifice conditions. For the 1.125 inch throat nozzle the uniform axial velocity was 25 feet per second, and the uniform axial velocity for the 2.0 inch nozzle was 85 feet per second. The tangential velocity was assumed to be a linear function of the radius with

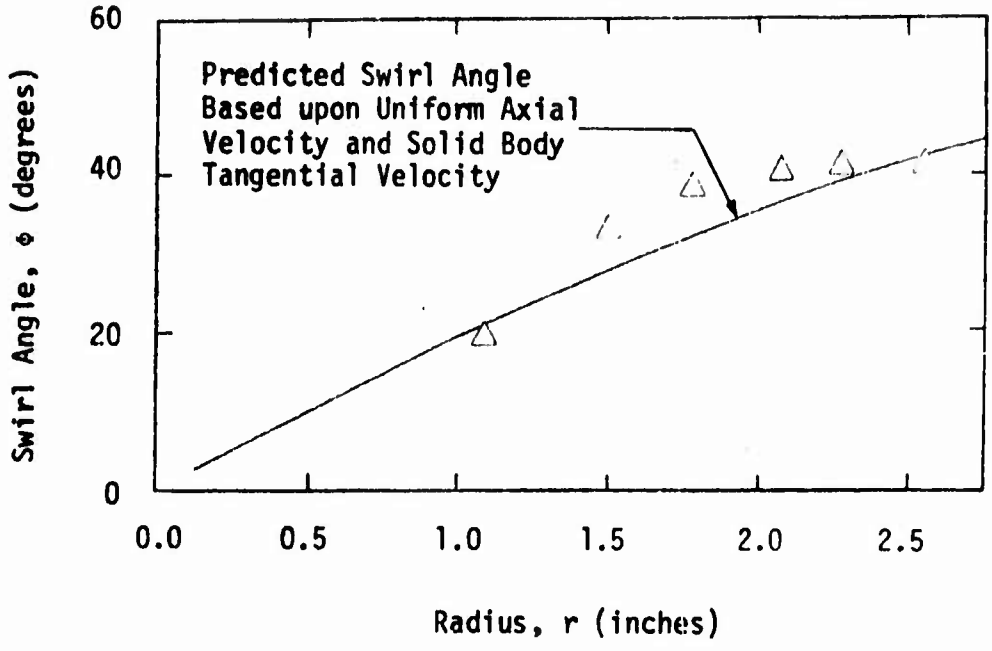

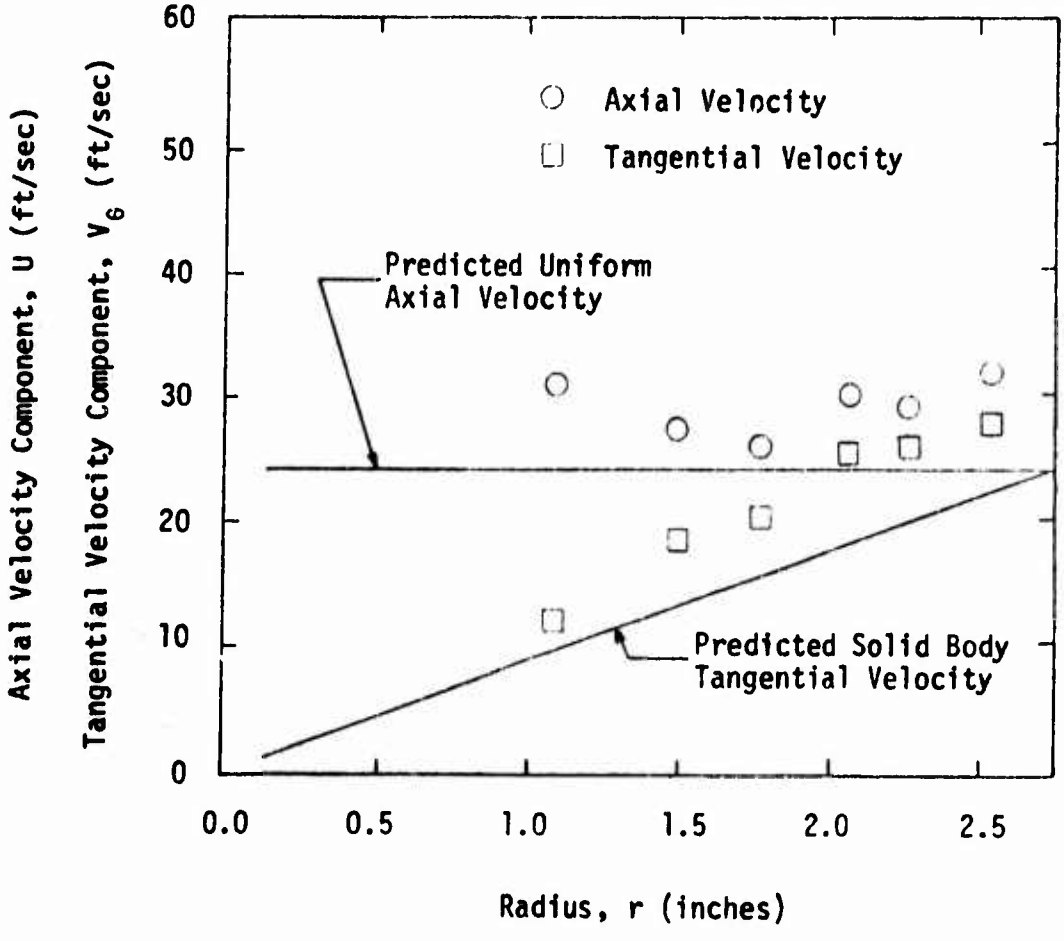

Figure 23 Swirl Angle and Velocity Profiles
1000 rpm ∿ 1.125 Inch Nozzle

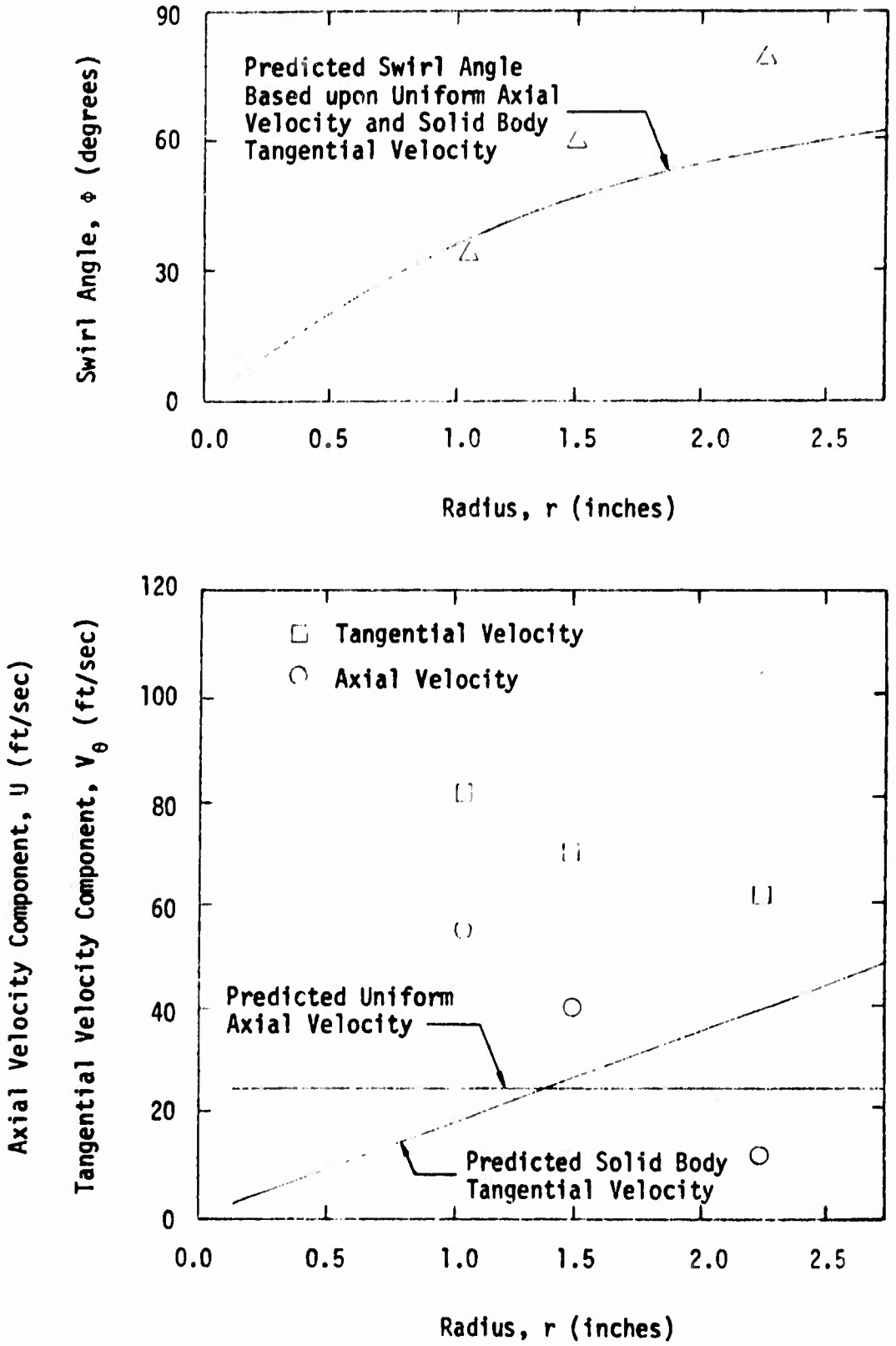

Figure 24 Swirl Angle and Velocity Profiles
2000 rpm ∿ 1.125 Inch Nozzle

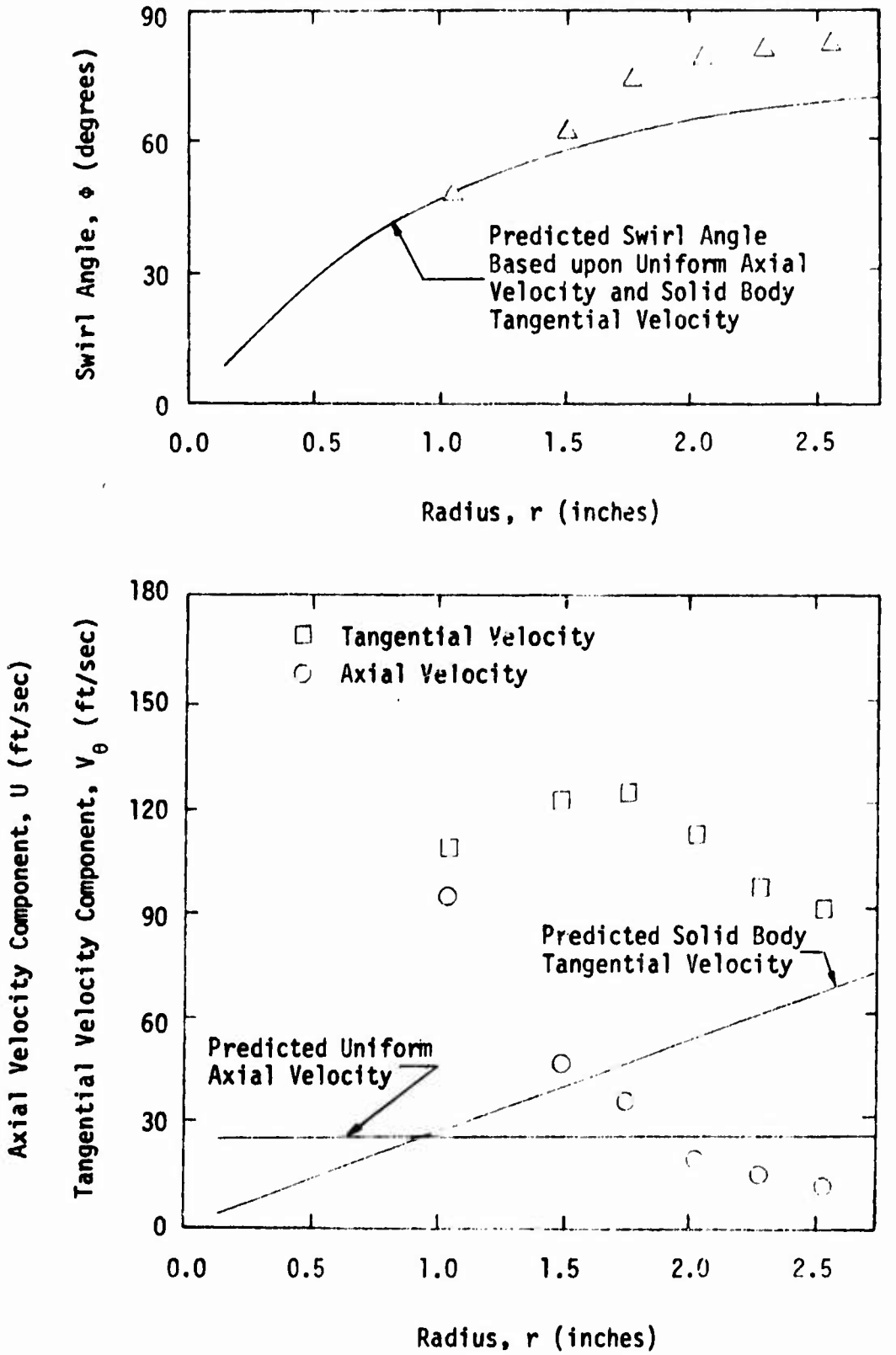

Figure 25 Swirl Angle and Velocity Profiles
3000 rpm ~ 1.125 Inch Nozzle

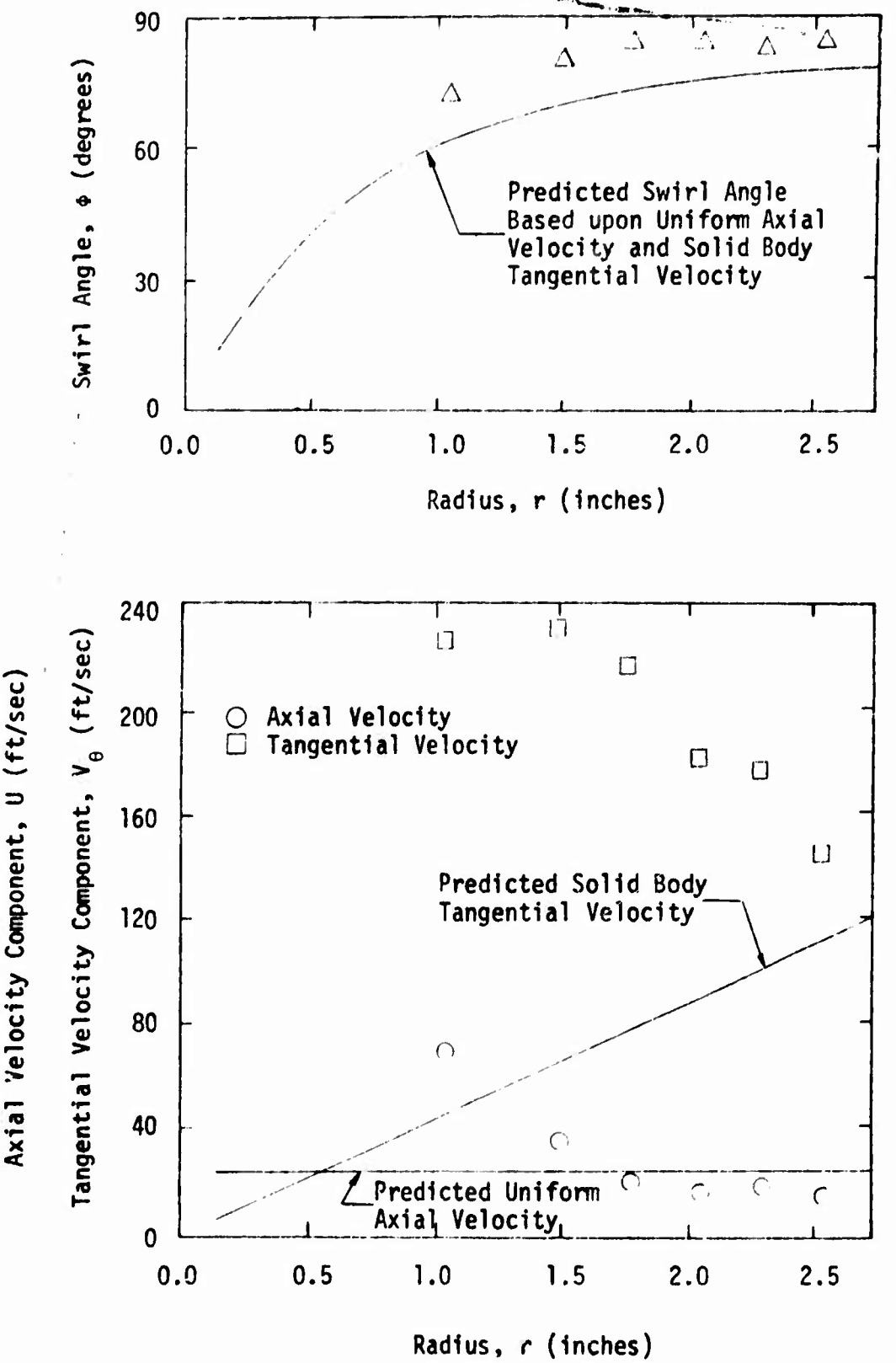

Figure 26 Swirl Angle and Velocity Profiles
5000 rpm ~ 1.125 Inch Nozzle

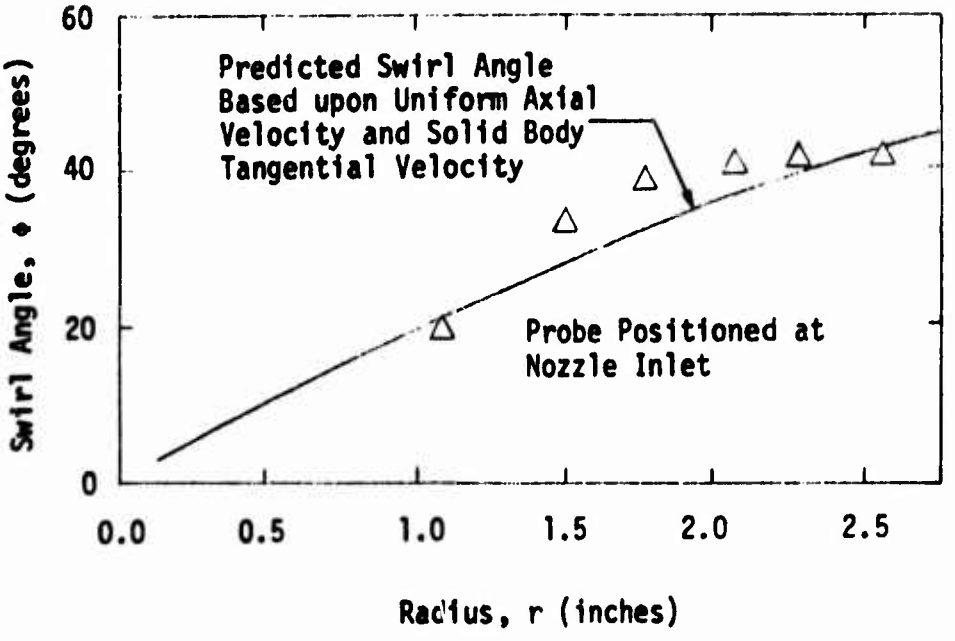

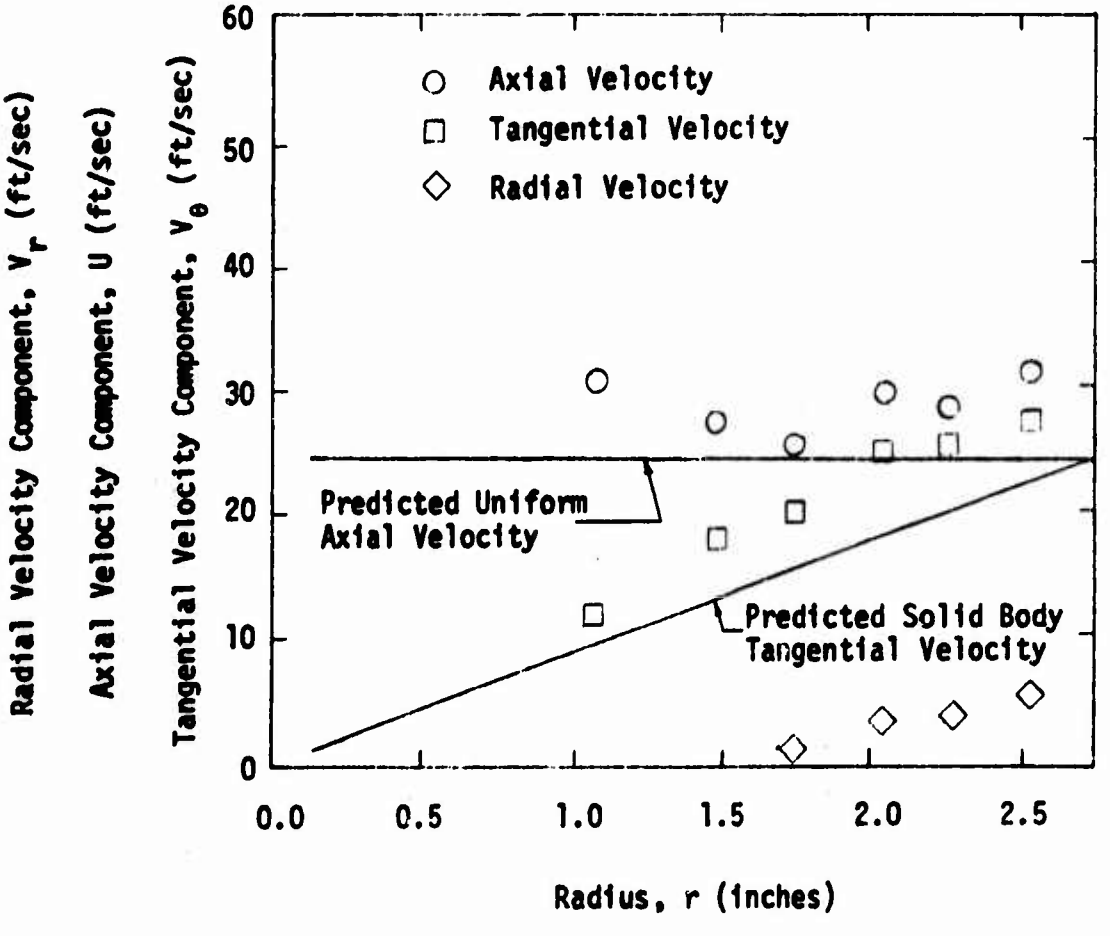

Figure 27 Swirl Angle and Velocity Profiles
1000 rpm ~ 1.125 Inch Nozzle

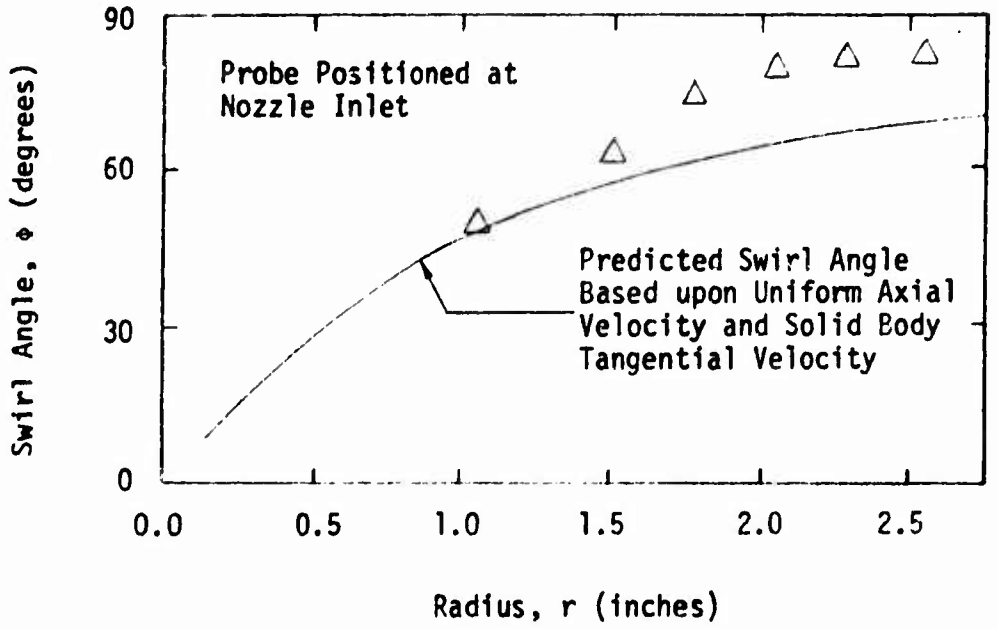

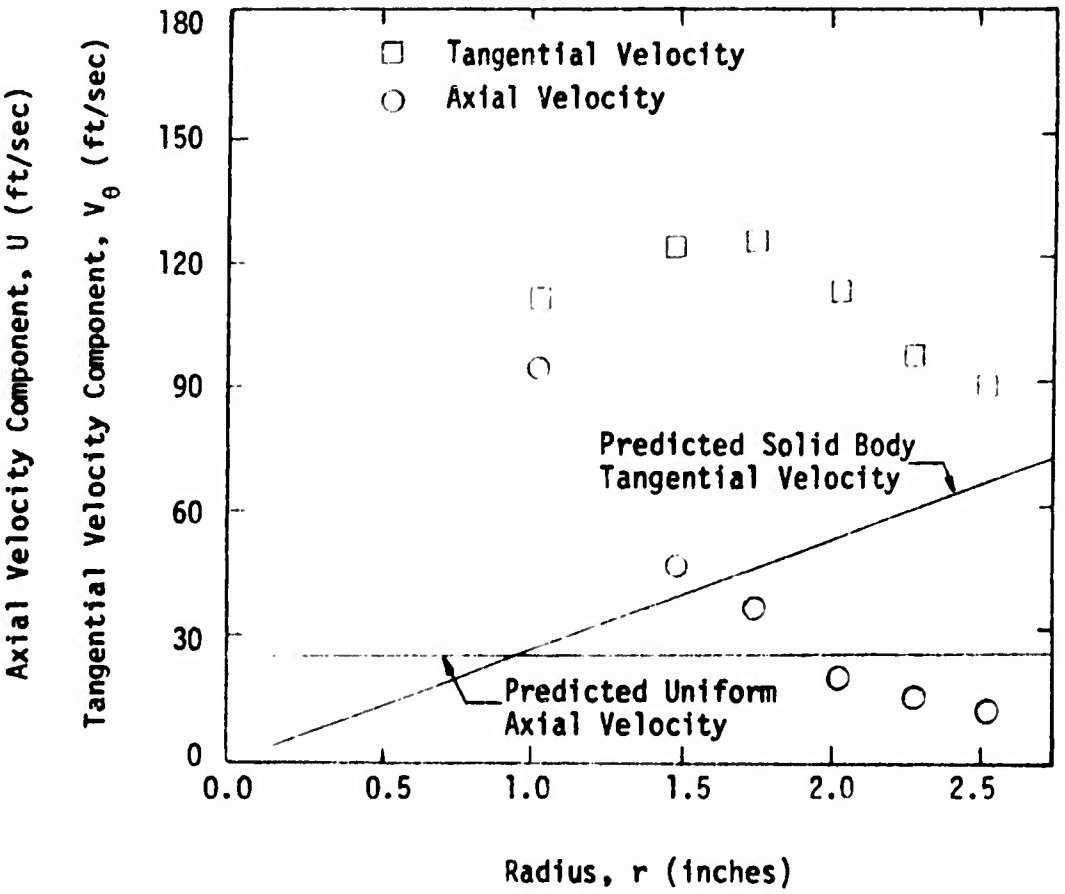

Figure 28 Swirl Angle and Velocity Profiles
3000 rpm ∿ 1.125 Inch Nozzle

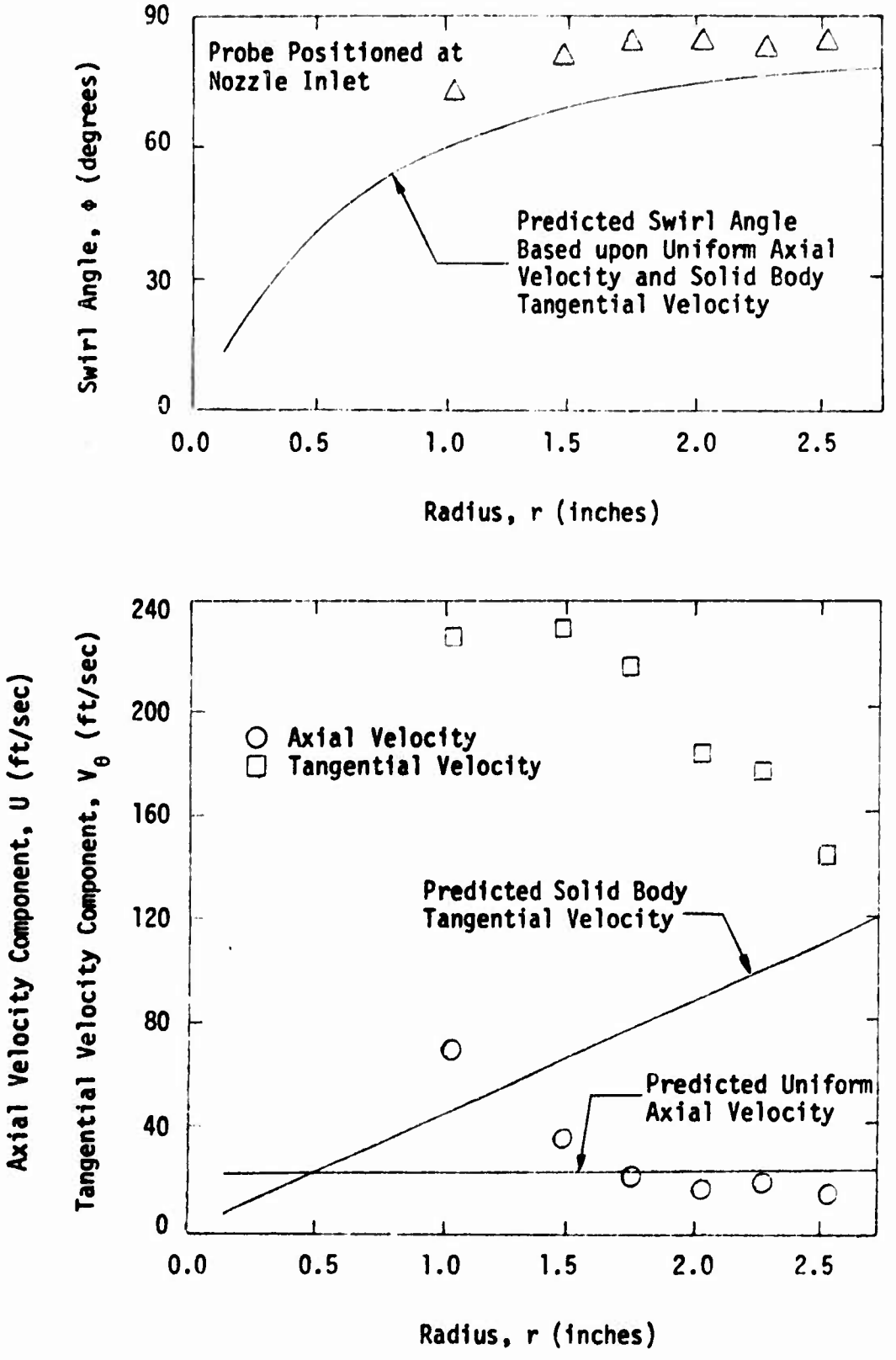

Figure 29 Swirl Angle and Velocity Profiles
5000 rpm ~ 1.125 Inch Nozzle

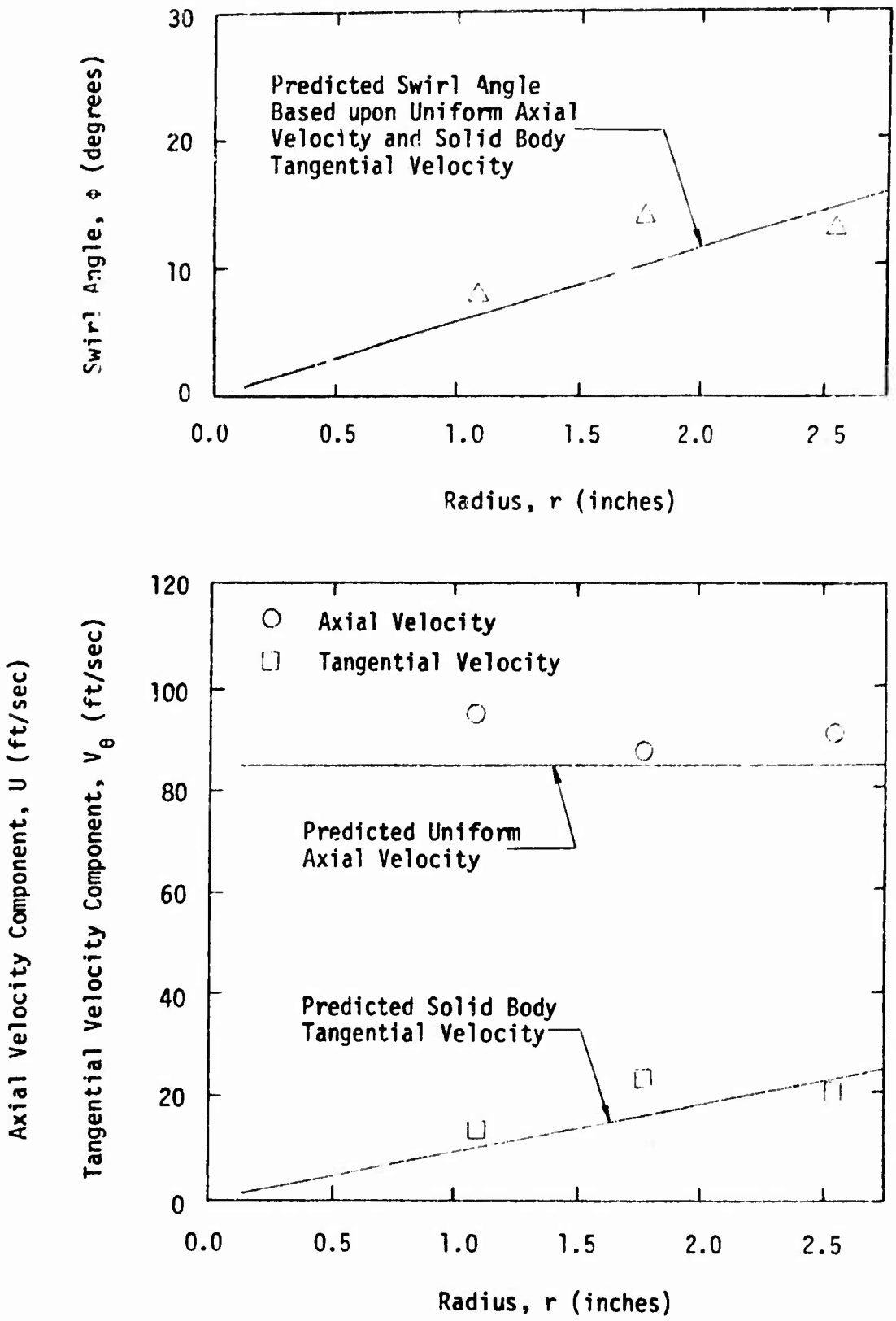

Figure 30 Swirl Angle and Velocity Profiles
1000 rpm ~ 2.0 Inch Nozzle

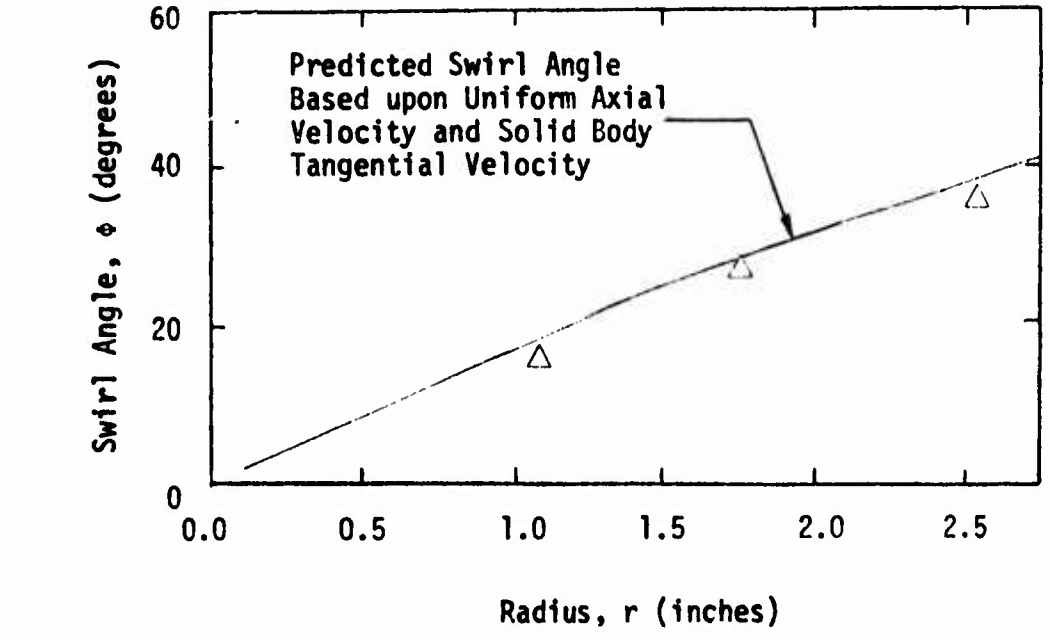

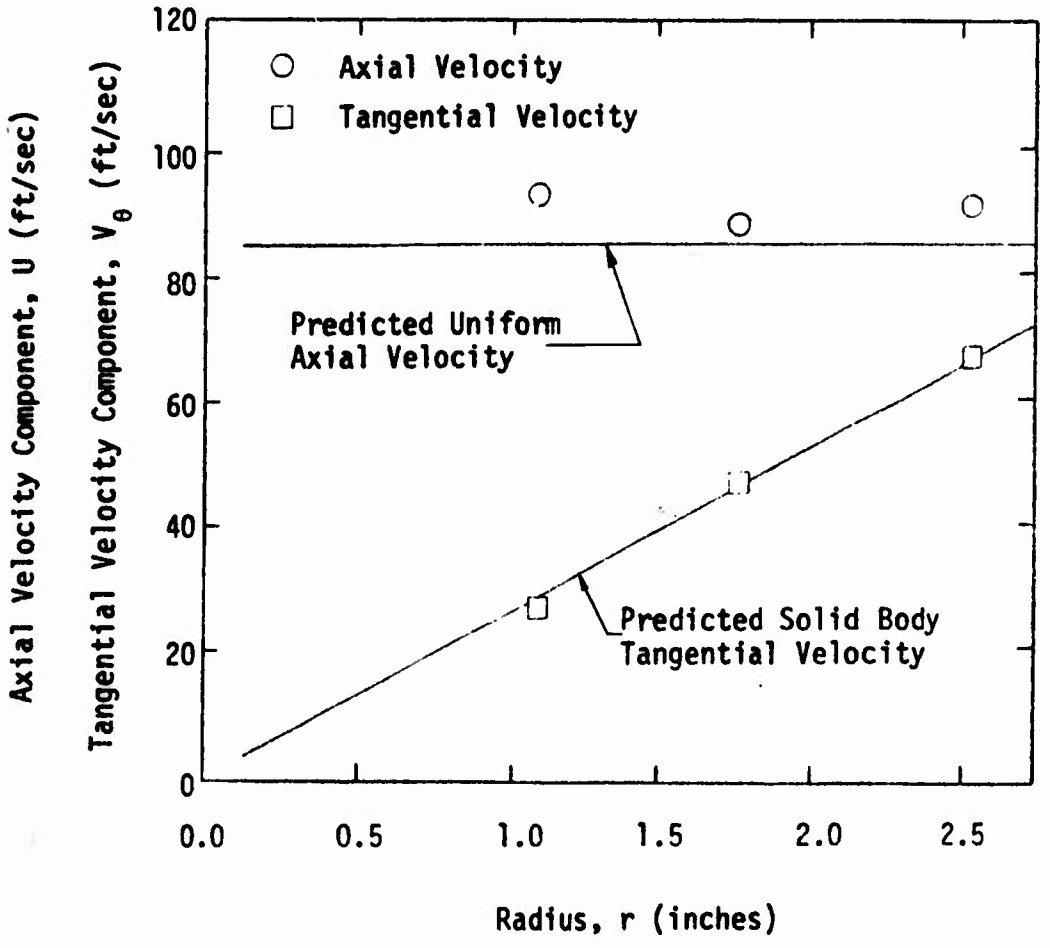

Figure 31 Swirl Angle and Velocity Profiles
3000 rpm ∿ 2.0 Inch Nozzle

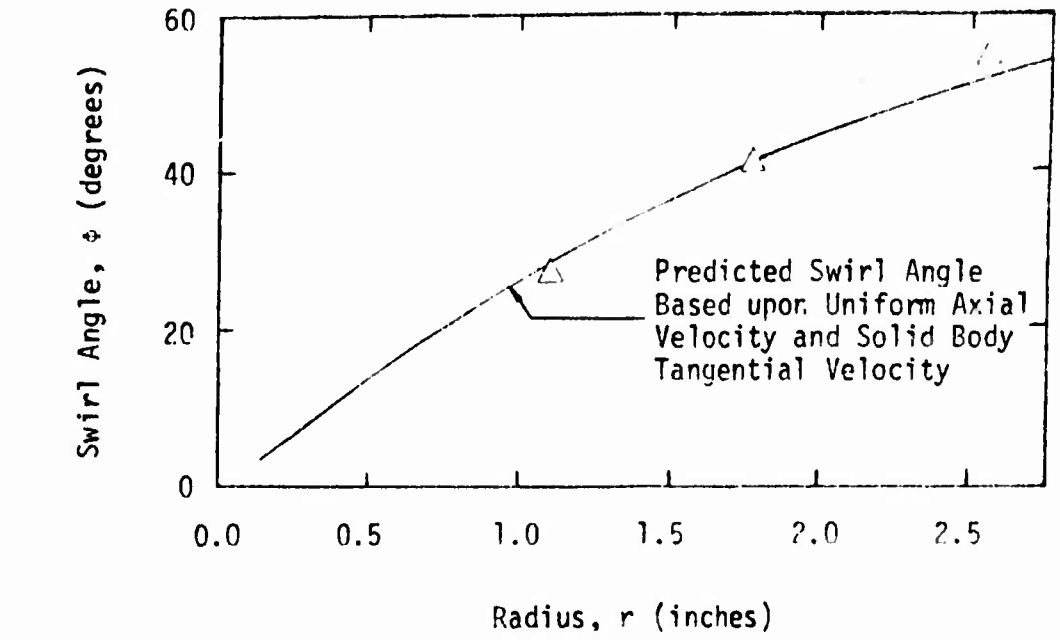

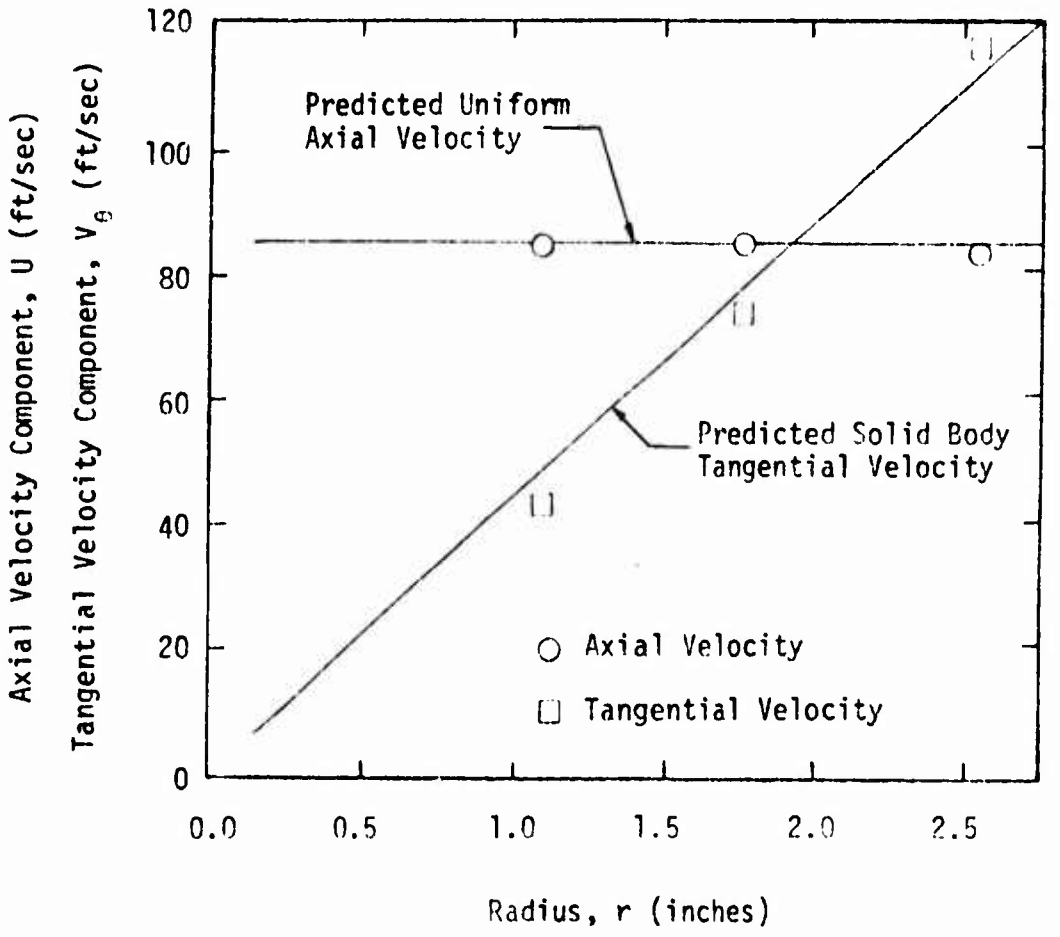

Figure 32 Swirl Angle and Velocity Profiles
5000 rpm ∿ 2.0 Inch Nozzle

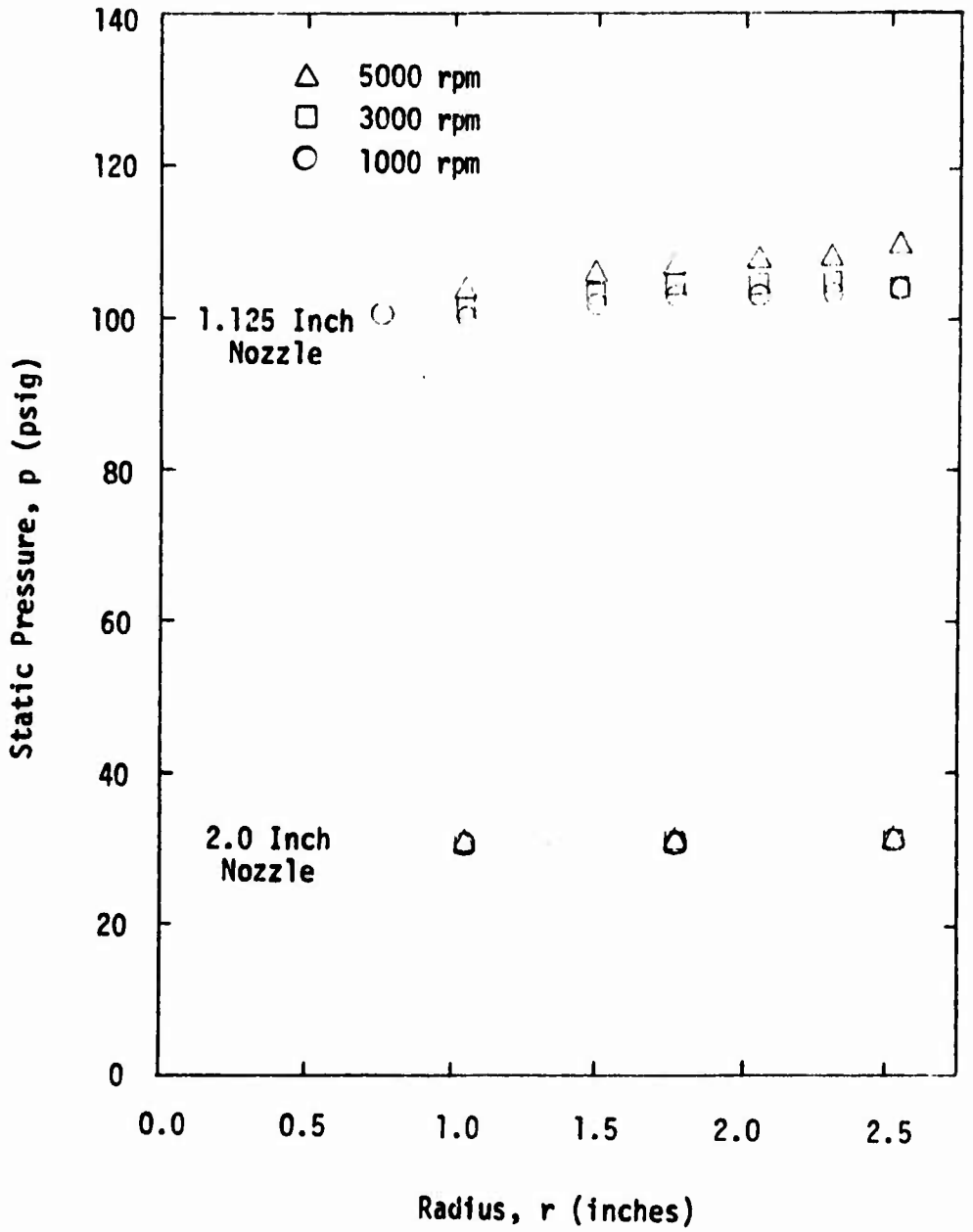

Figure 33 Static Pressure Profiles

the maximum tangential velocity equal to the chamber wall speed. The calculated swirl angle distribution was based on these assumed velocity profiles.

The velocity profiles shown in Figures 23, 27, 30, 31 and 32 exhibit trends similar to the assumed uniform axial velocity and solid body tangential velocity variations shown, whereas, the velocity profiles of Figures 24, 25, 26, 28 and 29 exhibit trends dissimilar to the assumed velocity variations. These results are discussed in detail in Section 5.1.

Figure 33 presents the static pressure profiles for the 1.125 inch throat nozzle and the 2.0 inch throat nozzle. The figure includes data for rotational speeds of 1000, 3000 and 5000 rpm for each nozzle.

5. DISCUSSION AND CONCLUSIONS

The five-port impact tube probe was used to measure the pressure and velocity distributions in the radial direction within the chamber of the spinning, cold-flow rocket motor. The results of the investigation are presented in Section 4.3. The significance of the experimental results and the conclusions are discussed in this chapter.

5.1 Discussion of the Results

The first series of tests were conducted in the rocket motor chamber utilizing the 1.125 inch throat diameter nozzle. These results are presented in Figures 23 through 29 and in Figure 33 in Section 4.3.

Figure 23 presents data for a rotational speed of 1000 rpm when the probe was positioned at the plane nearest the simulated end-burning grain. As can be seen, the swirl angle distribution compares within approximately 5 degrees or 17 per cent, to that expected for the solid body vortex with a uniform axial velocity. The measured axial velocity profile shown in Figure 23 was approximately constant within a range of ± 3 feet per second but the mean value was approximately 20 per cent larger than that calculated from the measured air mass flowrate. The measured tangential velocity variation exhibited a trend similar to that calculated for a solid body

vortex as shown in Figure 23 but the experimental values were approximately 25 per cent larger than the calculated tangential velocity distribution. Some of the scatter and deviation of the experimental results from the predicted values can be attributed to the limited accuracy of the measurements for flow velocities in the range of 25 feet per second as discussed in Section 4.1. The calibration data obtained at 100 feet per second were used for the data reduction which also introduces some inaccuracy. However, there is good general agreement of the experimental and predicted values thus confirming that at a rotational speed of 1000 rpm the simulated end-burning grain does provide a nearly uniform axial velocity and a tangential velocity varying directly with radius.

The results presented in Figures 24, 25 and 26 for rotational speeds of 2000, 3000 and 5000 rpm for the 1.125 inch throat diameter nozzle were contrary to what was expected for the simulated end-burning grain. The swirl angle, tangential velocity and the axial velocity distributions were significantly different from the distributions predicted for a uniform axial velocity and a solid body tangential velocity variation which are shown as solid lines in the figures. As can be seen in Figures 24, 25 and 26, the indicated experimental values of the swirl angle were larger, for the most part, than the calculated values based upon the assumed uniform axial velocity and solid body tangential velocity variations. In Figures 25 and 26, the 3000 and 5000 rpm data, the measured values of swirl angle were nearly constant at a value of 85 degrees.

In Figures 24, 25, and 26, the indicated tangential velocity variation more nearly varied inversely with radius (somewhat characteristic of a free vortex) rather than directly with radius (solid body vortex). The indicated axial velocity variation also differed from a uniform axial velocity profile. However, since large errors can be introduced in determining the axial velocity as the velocity increases and the swirl angle approaches 90 degrees, the deviation of the results for the indicated axial velocity may not be too significant.

The results of probing in the chamber when the probe was positioned at the inlet of the converging nozzle are presented in Figures 27, 28 and 29 for rotational speeds of 1000, 3000 and 5000 rpm, respectively. As can be seen by comparing the results for 1000 rpm, Figures 23 and 27, the tangential and axial velocities were identical within the accuracy of the measurements. Near the chamber wall, a small radial velocity of approximately 5 feet per second directed toward the motor centerline was observed. However, the important feature of Figure 27 was that the tangential velocity variation exhibited a trend similar to the predicted solid body tangential velocity variation. When the tangential velocity variations of Figures 25 and 28, for a rotational speed of 3000 rpm, were compared the results were again nearly identical but the results were contrary to what was expected. Figures 26 and 29, for a rotational speed of 5000 rpm, exhibit the same trends as the 3000 rpm data. Thus it can be seen that the results of probing in the chamber when the probe was

positioned at the inlet of the converging nozzle were similar to those observed at the injector plate when the 1.125 inch throat diameter nozzle was employed.

The preceeding results of probing, when the 1.125 inch throat diameter nozzle was employed, indicate that for a rotational speed of 1000 rpm the velocity variations were essentially that of a uniform axial velocity profile and a solid body tangential velocity profile. However, the velocity profiles for rotational speeds of 2000, 3000 and 5000 rpm did not exhibit these trends, but rather appeared somewhat characteristic of a free vortex. For rotational speeds greater than 1000 rpm, it appeared that either the probe was not sensing the true flow or a drastic alteration of the flow field had occurred.

To determine if the probe was sensing the true flow, an auxiliary investigation was conducted to determine if the velocity vector was truly included within the calibration range of the five-port impact tube probe. During this investigation it was found that the cone encompassing the calibration range of the probe was smaller in a swirling flow than in a uniform flow such as that employed in the calibration tunnel. The probe was originally calibrated in the calibration tunnel for a yaw angle range of ± 50 degrees. However, in the spinning cold-flow rocket motor, gradients in the flow field apparently reduced the range for accurate yaw angle determination to approximately ± 25 degrees. These results were obtained by conducting successive identical experimental runs with the probe positioned at various angular orientations as indicated in Figure 34. When the velocity vector was located between two adjacent probe settings such

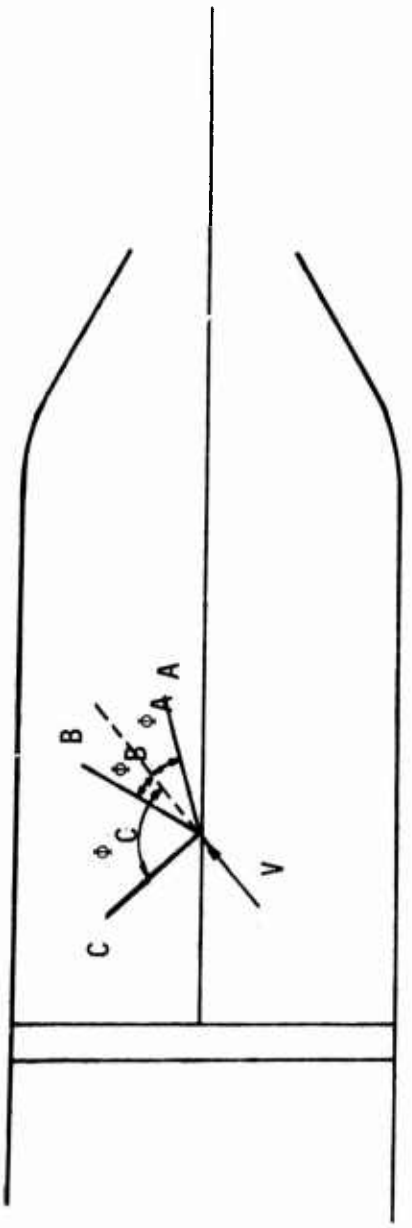

Figure 34 Probe Positions in the Cold-flow Apparatus

as "A" and "B" in Figure 34 and the angles ϕ_A and ϕ_B were less than 25 degrees, the flow parameters determined from the calibration charts for each probe position were found to be identical. Small differences in the flow parameters determined from the calibration charts were observed when the angle was greater than 25 degrees as illustrated by probe position "C" in Figure 34.

In referring back to the initial experimental data taken for the 1.125 inch nozzle, it was found that the angle between the probe and the velocity vector was always less than 25 degrees. Thus, for the data presented in Figures 23 through 29, it was concluded that the probe was sensing the flow as it existed with the probe present in the flow field.

The only apparent explanation for the deviation of the indicated tangential velocity variation from that for a solid body vortex was an alteration of the flow field downstream of the simulated end-burning grain.

Upon further examination, the results presented by Harvey (1962) (4) appeared to offer a possible explanation for a flow alteration in a swirling flow. Under certain conditions in his vortex tube experiments Harvey observed the formation of a closed "bubble" of recirculating fluid along the centerline of a vortex tube by employing smoke flow visualization techniques. Harvey's measurements indicated that the bubble diameter was approximately 20 per cent of the tube diameter. He noted that this bubble of fluid would form only when the conditions of the incoming fluid were such that the maximum swirl angle in the flow field was approximately 50 degrees, i.e., when the ratio of the

maximum tangential velocity to the axial velocity was approximately 1.2. As the inlet swirl angle was increased, the bubble would grow in length until eventually the entire length of the tube was filled with a bubble of recirculating fluid. Harvey observed that within this bubble, along the centerline, the axial velocity was in a direction opposite to that of the main flow down the tube; that is, the bubble contained a region in which the axial velocity was reversed. When the maximum swirl angle in the flow field was less than 50 degrees, formation of the bubble did not occur. But when the swirl angle was 50 degrees or larger, the bubble always formed along the centerline of the tube with an axial velocity reversal along the centerline. This result led Harvey to conclude that:

(1) the formation of the bubble was the bridge between the two types of vortex flow which have been used to characterize the swirling flow phenomena, i.e., a swirling flow with and without an axial velocity reversal as discussed in Section 1.1.

(2) and that the formation of the bubble was primarily associated with the single parameter, $(V_\theta)_{max}/U$.

Harvey also observed a second significant feature of the flow. He found that when a small bubble was formed ($(V_\theta)_{max}/U$ of approximately 1.2) that the entire flow field was hypersensitive to a flow disturbance. This was so serious that a probe introduced a little upstream of the bubble produced enough interference to produce a second bubble upstream of the probe. The hypersensitivity to a flow disturbance and the bubble diameter of approximately 20 per cent of the tube diameter could explain the difficulty, on which previous

investigators have commented, in obtaining reproducible measurements near the centerline of a vortex tube.

When the present results of probing in the chamber (1.125 inch throat diameter nozzle) were examined in the light of Harvey's results, an interesting point was noted. For the predicted solid body tangential velocity distribution and uniform axial velocity distribution, the maximum value of V_θ/U occurs at the wall. For a rotational speed of 1000 rpm, the predicted value of $(V_\theta)_{max}/U$ was 1.0. The experimental data presented in Figure 23 also indicated a value of $(V_\theta)_{max}/U$ of approximately 1.0. For a rotational speed of 2000 rpm, the predicted value of $(V_\theta)_{max}/U$ was 2.0. However, it will be recalled that the experimental results for a rotational speed of 2000 rpm showed a marked change in the tangential velocity variation from that expected for a solid body variation. These results indicated that the deviation from the solid body velocity variation occurred at a rotational speed between 1000 rpm and 2000 rpm, which corresponded to a value of $(V_\theta)_{max}/U$ between 1.0 and 2.0. Since this range of $(V_\theta)_{max}/U$ encompassed Harvey's result of 1.2 for the bubble formation and flow hypersensitivity, it was thought that some type of flow alteration, perhaps similar to that observed by Harvey, might explain the deviation from the solid body variation observed for rotational speeds of 2000, 3000 and 5000 rpm.

At this stage of the investigation, the dependence of the flow field on the parameter $(V_\theta)_{max}/U$ could not be confirmed with any degree of certainty. However, if this criterion could be used to

characterize the nature of the flow in the spinning, cold-flow rocket motor, increasing the axial velocity in the chamber should allow higher rotational speeds to be attained before a deviation from the solid body velocity variation is observed.

This result prompted the study employing the larger, 2.0 inch throat diameter nozzle. For the 2.0 inch nozzle the chamber axial velocity based on the air mass flowrate was 85 feet per second. Measurements were conducted at rotational speeds of 1000, 3000 and 5000 rpm to determine the shape of the tangential velocity profile when the 2.0 inch diameter nozzle was employed.

Figures 30, 31 and 32 present data for the 2.0 inch throat diameter nozzle for rotational speeds of 1000, 3000 and 5000 rpm, respectively. The probe was positioned at the plane nearest the simulated end-burning grain. Again, the solid lines represent the predicted tangential velocity component, the axial velocity component and the swirl angle for reference. As can be seen, the velocity and swirl angle variations shown are similar to the results expected for a uniform axial velocity and a solid body tangential velocity variation. The swirl angle distribution shown in Figure 30 compares within approximately 4 degrees or approximately 35 per cent to that expected for the solid body vortex and a uniform axial velocity. The measured axial velocity shown in Figure 30, for a rotational speed of 1000 rpm, was approximately constant within a range of ± 3 feet per second with the mean value approximately 7 per cent larger than the uniform axial velocity calculated from the air mass flowrate. The measured tangential velocity variation was within ± 5 feet per second or approximately

35 per cent of the predicted tangential velocity based on a solid body variation. The swirl angle measurements and the tangential velocity variations shown in Figure 31, for a rotational speed of 3000 rpm, agree quite favorably with the predicted values. The measured mean axial velocity shown in Figure 31 was again within 7 per cent of the calculated axial velocity. The swirl angle, tangential velocity and axial velocity variations shown in Figure 32, for a rotational speed of 5000 rpm, once again agree quite favorably with the predicted values. For this case, the measured axial velocity was within 1 per cent of the calculated axial velocity.

The results of probing in the chamber when the 2.0 inch diameter nozzle was employed indicated that for rotational speeds up to 5000 rpm the tangential velocity variation was characteristic of a solid body vortex. Whereas, for the 1.125 inch nozzle, the tangential velocity variation retained a solid body character only up to a rotational speed of 1000 rpm.

In view of the preceding results, it was desired to determine if the tangential velocity variation, when the 2.0 inch nozzle was employed, would be altered in a similar manner to that observed for the 1.125 inch nozzle. An experiment was conducted to investigate the nature of the profiles as the rotational speed was increased above 5000 rpm.

For this experiment, the probe was positioned in the chamber at a 1.1 inch radius. This radial position was selected on the basis of the data presented in Figures 23, 24 and 25. In referring to Figures 23, 24 and 25, it can be seen that the deviation in the

measured tangential velocity and the predicted solid body tangential velocity was most pronounced at this radius.

The results of the experiment are presented in Table 1. At 5000 rpm the measured tangential velocity was 43 feet per second and the measured axial velocity was 85 feet per second. These results were in excellent agreement with the predicted tangential and axial velocity, indicating that for a rotational speed of 5000 rpm, the tangential velocity distribution was characteristic of a solid body vortex. However, at 6000 rpm the measured tangential velocity was 150 feet per second and the measured axial velocity was 101 feet per second, as compared with the predicted velocities of 52 feet per second and 85 feet per second, respectively. These results indicated that for a rotational speed of 6000 rpm, the tangential velocity was no longer a solid body variation. From the data for a rotational speed of 5500 rpm, it was difficult to determine which profile shape was present. However, it appeared that a deviation from the expected solid body tangential velocity profile definitely occurred between rotational speeds of 5500 rpm and 6000 rpm. These speeds correspond to a predicted value of $(V_\theta)_{max}/U$ between 1.56 and 1.70.

The results of probing when the 2.0 inch nozzle was employed provided additional experimental evidence of the dependence of the nature of the flow field on the parameter $(V_\theta)_{max}/U$. This similarity between the results of the subject investigation and Harvey's result was striking, although it could not be concluded that the phenomena were necessarily the same.

TABLE 1

Tabular Data
2.0 Inch Throat Diameter Nozzle

	Manometer Readings			From Calibration Charts			Predicted Data		
RPM	$P_1 - P_3$ (mm H_g)	$P_2 - P_4$ (mm H_g)	$P_5 - P_1$ (mm H_g)	ϕ (deg)	V_θ (ft/sec)	U (ft/sec)	ϕ (deg)	V_θ (ft/sec)	U (ft/sec)
1000	0.0	- 25	+12	8	13	91	6.5	10	85
3000	0.0	- 14	+12	16	27	91	18.5	29	85
5000	0.0	- 6	+13	27	43	85	29.5	48	85
5500	0.0	+ 7	+14	38	68	89	32	53	85
6000	0.0	+ 71	+30	56	150	101	34	58	85
7000	0.0	+188	+63	64	230	117	38	68	85

At the present time the only apparent explanation for the profile shape observed when $(V_\theta)_{max}/U$ was greater than approximately 1.6, is the hypersensitivity of a swirling flow to a flow disturbance. Obviously, the presence of the probe and traversing mechanism in the flow field perturbs the flow. Therefore it appears that the explanation for the trend of the results presented in Figures 23, 24, 25, 27 and 28 could be any of the following:

(1) At a tangential to axial velocity ratio of approximately 1.6, the flow cannot sustain the probe perturbation and the probe disrupts the entire flow field due to its presence. The indicated profiles are not representative of the flow field without the probe present;

(2) Or, at each radial position the probe senses a local flow perturbation due to the presence of the probe, and the indicated profiles are not representative of the entire flow field;

(3) Or, the profiles measured are representative of the flow field in the chamber.

A suitable explanation will apparently require a non-perturbing probing technique, such as flow visualization or the laser velocimeter. As mentioned in Section 1.3, the impact tube probe was the only practical technique for this study and the results must, therefore, be considered inconclusive for the flow field measurements when the ratio of maximum tangential velocity to axial velocity was 1.6 or greater.

Figure 33 presents the static pressure measurements as a function of radius for both the 1.125 inch nozzle and the 2.0 inch nozzle at rotational speeds of 1000, 3000 and 5000 rpm. As can be seen, the static pressure was nearly constant across the motor radius. The relationship for the radial pressure gradient for an inviscid fluid with a uniform axial velocity and a solid body tangential velocity is:

$$\frac{dp}{dr} = \rho r \omega_o^2 \tag{5.1}$$

Integrating 5.1 for a constant density, the pressure change from the centerline to the wall is given by:

$$\Delta p = \frac{1}{2}\rho \left(R_w \omega_o\right)^2 \tag{5.2}$$

where $R_w \omega_o$ is the tangential velocity at the wall. The pressure change calculated for the 1.125 inch nozzle at 5000 rpm was approximately 1.0 psi and for the 2.0 inch nozzle, at 5000 rpm, approximately 0.25 psi. These calculations indicate that for rotational speeds less than 5000 rpm, the static pressure is nearly constant which is in agreement with the experimental observations.

5.2 Conclusions

While the experimental program reported herein needs extension for a complete understanding of the phenomena occurring, some conclusions may be stated concerning the probing of the flow field within the chamber of the spinning, cold-flow rocket motor.

From a review of the findings, the following conclusions may be stated:

(1) Two distinct velocity profiles were observed. The first type was essentially a uniform axial velocity and a solid body tangential velocity variation. The second type observed was more similar to a free vortex. The deviation from the solid body variation occurred when the ratio of the maximum solid body tangential velocity to the axial velocity was approximately 1.6, i.e., a swirl angle of 57 degrees.

(2) The results were inconclusive for the profile shape for swirl angles greater than 57 degrees.

(3) The velocity profiles at the nozzle were similar to those observed at the injector plate.

(4) No evidence of an axial velocity reversal was observed.

(5) The radial pressure gradient for rotational speeds less than 5000 rpm was negligible.

(6) The five-port impact tube probe provided results in good agreement with the results expected for the rotating flow with a swirl angle less than 57 degrees.

(7) The useable calibration range for the five-port impact tube probe was found to be reduced to approximately ± 25 degrees (yaw angle) in a swirling flow.

(8) A complete probe calibration, that is, the ability to make measurements in a three-dimensional flow with a fixed probe,

is laborious, but once completed, the time required to obtain results is reasonable.

In closing, it seems appropriate to examine the possible significance of the results presented herein in the development of a better understanding of the interior ballistics of spinning, solid propellant rocket motors. Previous examinations of partially burned end-burning solid propellant grains, after spin test, have revealed the existence of a shallow cone-shaped depression in the center of the burning surface. This "coning" of the propellant surface can be attributed to some cause for an increased burning rate at that point. One explanation which has been offered for this coning phenomenon is the possibility of an erosive burning effect due to the presence of a reversed flow region along the motor centerline with the impingement of hot gases on the burning surface. This postulated mechanism is based upon the experimental observation in vortex tubes, under certain conditions, of regions of reversed flow as reported by Harvey and many others. Unfortunately, the tests with interrupted firings of solid propellant rocket motors have not been extensive enough to determine whether there is a lower limit of the spin rate below which the coning phenomenon is not observed.

It would be of considerable interest to conduct a series of hot-firing, spin tests of a group of identical end-burning solid propellant rocket motors. The propellant should be selected to provide the largest chamber axial velocity possible. The motors should be fired while being spun at constant values of the spin rate. Tests

should be conducted at values of the spin rate selected so that the maximum tangential velocity is less than, approximately equal to, and greater than the chamber axial velocity. It would be necessary to interrupt each hot firing in order to examine the burning surface for the existence of coning. Experimental results of this type should enhance the understanding of the interior ballistics of spinning, solid propellant rocket motors.

BIBLIOGRAPHY

1. Norton, D. J., Farquhar, B. W., and Hoffman, J. D., "Analytical Studies of the Interior Ballistics of Spinning Rocket Motors - A Literature Survey," Purdue Univ., Jet Propulsion Center Report No. TM-67-1, January 1967.

2. Norton, D. J., Farquhar, B. W., and Hoffman, J. D., "An Analytical Investigation of the Fluid Mechanics of Rotating Flows in Rocket Motors," Purdue Univ., Jet Propulsion Center Report No. TM-67-7, October 1967.

3. Farquhar, B. W., Norton, D. J., and Hoffman, J. D., "An Experimental Investigation of Swirling Flow in Nozzles," Purdue Univ., Jet Propulsion Center Report No. TM-67-8, January 1968.

4. Harvey, J. K., "Some Observations of the Vortex Breakdown Phenomenon," Journal of Fluid Mechanics, Volume 14, Part 4, December 1962.

5. Youseff, T. E., "Some Investigations on the Rotating Flow with a Recirculation Core in Straight Pipes," ASME Preprint 66-WA/FE-36, December 1966.

6. Eckert, E. R. G. and Hartnet, J. P., "Measurements of the Energy Separation in a High Velocity Vortex Flow," Stanford Univ., Heat Transfer Institute Conference, June 1956.

7. Hartnett, J. P. and Eckert, E. R. G., "Experimental Study of the Velocity and Temperature Distribution in a High Velocity Vortex Type Flow," Stanford Univ., Proceedings of Heat Transfer and Fluid Mechanics Institute, 1956.

8. Lay, J. E., "An Experimental and Analytical Study of Vortex Flow Temperature Separation by Superposition of Spiral and Axial Flows, Parts I and II," Transactions of the ASME, Journal of Heat Transfer, August 1959.

9. Farquhar, B. W., Norton, D. J., and Hoffman, J. D., "Investigation of High Acceleration on the Interior Ballistics of Solid Propellant Rocket Motors," Purdue Univ., Jet Propulsion Center Report No. F-66-10, December 1966.

10. Winternitz, F. A. L., "Probe Measurements in Three-dimensional Flow," Aircraft Engineering, August 1956.

11. Bryer, D. W., Halshe, D. E., and Garner, H. C., "Pressure Probes Selected for Three-dimensional Flow Measurement," National Physics Laboratory, Reports and Memoranda 3037, November 1955.

12. Ash, J. E. and Lee, J. C., "A Three-dimensional Spherical Pitot Probe," ASME Preprint 55-SA-56, April 1955.

APPENDIX A

CALIBRATION SCHEME

The coordinate system, flow angle definitions and an illustration of the probe tip are shown in Figure A.1 as reference for the following discussion of the calibration scheme.

The pressures read in each port, p_n, can be written as the static pressure, p, plus some fraction of the dynamic pressure, $K_n q$, as follows:

$$p_n = p + K_n q \tag{A.1}$$

where the subscript n refers to the n^{th} port, K_n is the calibration factor for the correspondingly numbered port and q is the dynamic pressure ($\frac{1}{2}\rho V^2$). For low speed flow K_n is a function of the probe geometry and the probe orientation with respect to the flow direction. The pitch ports are numbered 1 and 3 and the yaw ports are designated 2 and 4. The central port is port 5. By combining the pressure equations A.1 for each of the five ports, the following ratios are obtained:

$$\frac{p_1 - p_3}{p_5 - p_1} = \frac{K_1 - K_3}{K_5 - K_1} = f_1(\theta,\psi) \tag{A.2}$$

and

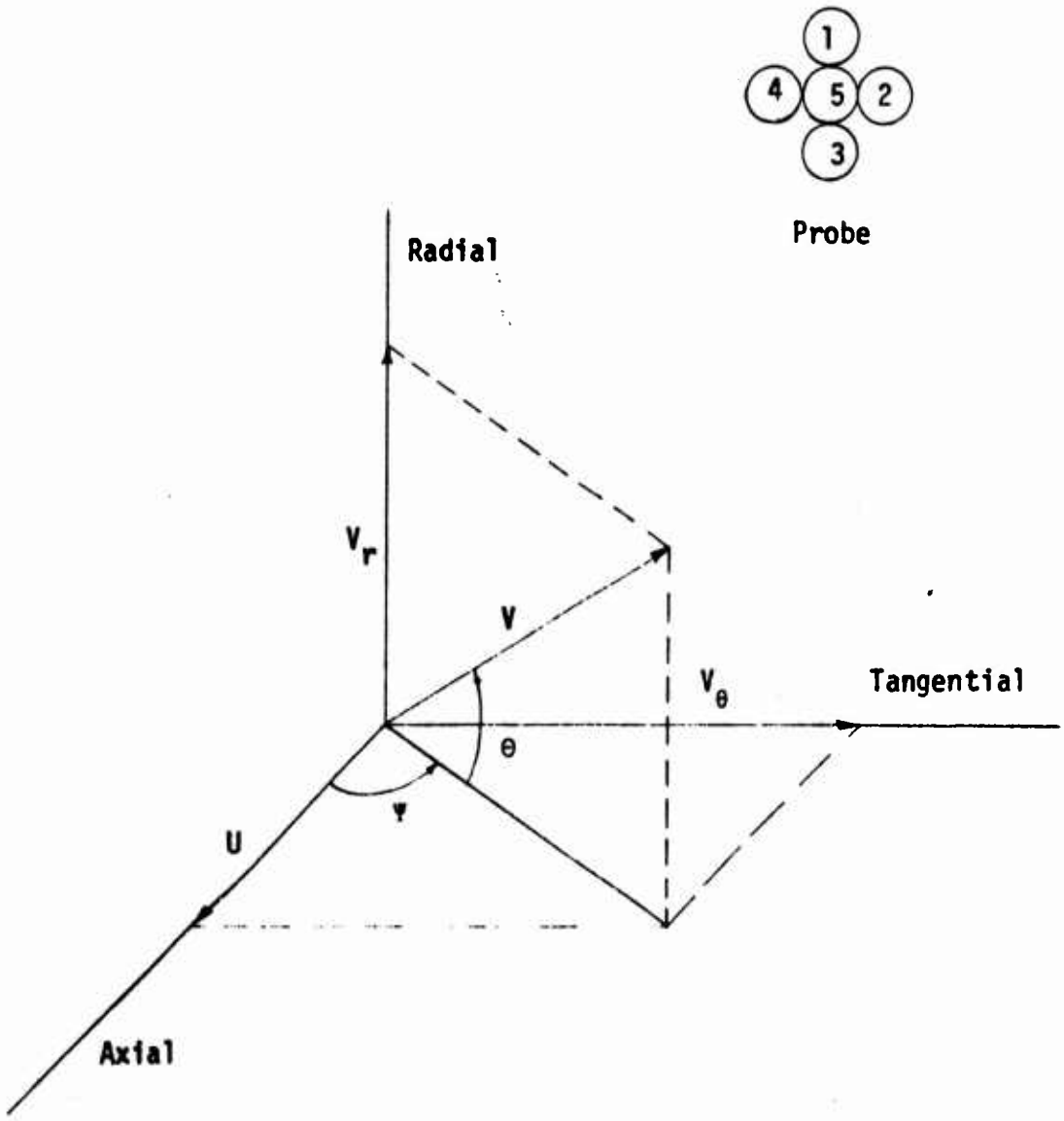

Figure A1 Coordinate System

$$\frac{p_2 - p_4}{p_5 - p_1} = \frac{(K_2-K_4)}{(K_5-K_1)} = f_2(\theta,\psi) \qquad (A.3)$$

For a given probe configuration, these ratios are only functions of the flow angles θ and ψ.

In a similar manner, from the pressure equation A.1 the following relationship is formed:

$$\frac{p_1 - p_3}{q} = K_1 - K_3 = f_3(\theta,\psi) \qquad (A.4)$$

For low Mach numbers the flow is nearly incompressible and

$$H = p + q \qquad (A.5)$$

where H is the total pressure. For the central port, equation A.5 and A.1 can be combined to form the following relationship:

$$H = p_5 + (1-K_5)q \qquad (A.6)$$

or letting $K_5' = 1 - K_5$

$$H = p_5 + K_5'q \qquad (A.7)$$

Thus, the total pressure is the sum of the pressure in the central port plus some fraction of the dynamic pressure. Rearranging A.7

$$\frac{H - p_5}{q} = K_5' = f_4(\theta,\psi) \qquad (A.8)$$

Each of the functions A.2, A.3, A.4 and A.8 can be determined experimentally, for a given probe configuration, by measuring the

pressure differences between the corresponding ports on the probe for a known orientation of the probe with respect to the free stream velocity vector. The two functions A.2 and A.3 give θ and ψ which determine the direction of the velocity vector. Knowing θ and ψ the dynamic pressure, q, can be determined from A.4. The total pressure, H, can then be determined from A.8 since θ, ψ and q are known. The static pressure, p, is determined from A.5 and with a suitable temperature the density can be calculated and the flow velocity found from the definition of the dynamic pressure

$$V = \sqrt{\frac{2q}{\rho}} \tag{A.9}$$

The temperature used in determining the air density was the orifice static temperature. Since the velocity is a function of the square root of the temperature and the fluid was air at approximately 500 degrees Rankine, a temperature change from the orifice to the chamber of 20 degrees Rankine would result in only a 2 per cent error in velocity magnitude. This approximation appeared reasonable and eliminated temperature measurements within the chamber.

TABLE B1

Tabular Data

1000 rpm ~ 1.125 Inch Nozzle

r (in)	Probe	p_1-p_3 (mm Hg)	p_2-p_4 (mm Hg)	p_5-p_1 (mm Hg)	p_5 (psig)	T (R)	Ψ (deg)	θ (deg)	U (fps)	V_θ (fps)	V_r (fps)
2.55	I.P.	0	-5	6.5	108	470	41	0	32	28	0
2.30	I.P.	0	2.5	5.5	107	460	42	0	29	26	0
2.07	I.P.	0	-5	6.5	106	470	41	0	30	25	0
1.77	I.P.	0	-2.5	4.0	107	460	39	0	26	21	0
1.50	I.P.	0	-2.5	4.0	105	470	33	0	28	18	0
1.11	I.P.	0	-2.5	4.0	101	460	19	0	31	11	0
2.55	N.I.	2.5	-5	6.5	107	470	41	8	32	28	6
2.30	N.I.	1.5	2.5	5.5	107	460	42	6	29	26	4
2.07	N.I.	1.5	-5	6.5	106	470	41	4	30	25	3
1.77	N.I.	0.5	-2.5	4.0	107	460	39	2	26	21	1
1.50	N.I.	0	-2.5	4.0	105	470	33	0	28	18	0
1.11	N.I.	0	-2.5	4.0	100	460	19	0	31	11	0

TABLE B2

Tabular Data
3000 rpm ~ 1.125 Inch Nozzle

r (in)	Probe	p_1-p_3 (mm Hg)	p_2-p_4 (mm Hg)	p_5-p_1 (mm Hg)	p_5 (psig)	T (R)	ψ (deg)	U (fps)	V_θ (fps)
2.55	I.P.	0	48	29	107	470	82	11	90
2.30	I.P.	0	-47	33	108	460	81	15	98
2.07	I.P.	0	44	37	107	470	79	19	112
1.77	I.P.	0	86	43	107	460	74	36	124
1.50	I.P.	0	-41	43	106	470	63	47	121
1.11	I.P.	0	43	47	102	460	48	94	109
2.55	N.I.	0	47	29	107	470	82	11	89
2.30	N.I.	0	-48	33	107	460	81	15	98
2.07	N.I.	0	44	37	107	470	79	19	112
1.77	N.I.	0	86	43	106	460	74	36	124
1.50	N.I.	0	-42	43	104	470	63	46	121
1.11	N.I.	0	43	48	101	460	48	93	110

TABLE B3

Tabular Data
5000 rpm ~ 1.125 Inch Nozzle

r (in)	Probe	P_1-P_3 (mm Hg)	P_2-P_4 (mm Hg)	P_5-P_1 (mm Hg)	P_5 (psig)	T (R)	ψ (deg)	U (fps)	V_θ (fps)
2.55	I.P.	0	28	47	110	470	85	14	145
2.30	I.P.	0	37	58	110	460	84	17	177
2.07	I.P.	0	46	60	110	470	85	15	182
1.77	I.P.	0	93	71	109	460	85	20	217
1.50	I.P.	0	51	77	108	470	81	35	234
1.11	I.P.	0	42	77	104	460	72	70	227
2.55	N.I.	0	27	46	110	470	85	14	144
2.30	N.I.	0	37	58	109	460	84	17	177
2.07	N.I.	0	45	60	109	470	85	15	180
1.77	N.I.	0	93	71	108	460	85	20	217
1.50	N.I.	0	51	77	107	470	81	35	234
1.11	N.I.	0	42	77	104	460	72	70	227

TABLE B4

Tabular Data
2.0 Inch Nozzle

rpm	r (in)	p_1-p_3 (mm Hg)	p_2-p_4 (mm Hg)	p_5-p_1 (mm Hg)	p_5 (psig)	T (R)	ψ (deg)	U (fps)	V_θ (fps)
1000	2.55	0	-17	24	30	490	13	90	21
1000	1.77	0	-10	20	30	480	14	88	22
1000	1.11	0	-25	12	30	495	8	94	13
3000	2.55	0	5	28	30	490	38	89	67
3000	1.77	0	.1	23	30	480	27	87	48
3000	1.11	0	-14	12	30	495	16	91	27
5000	2.55	0	39	35	30	490	57	83	117
5000	1.77	0	14	23	30	480	41	85	74
5000	1.11	0	-6	13	30	495	27	85	43